Submitted to Progress in Quantum Electronics

LBL-3114
Preprint c.2

FAR-INFRARED GENERATION BY OPTICAL MIXING

Y. R. Shen

July, 1974

Prepared for the U. S. Atomic Energy Commission
under Contract W-7405-ENG-48

TWO-WEEK LOAN COPY

This is a Library Circulating Copy which may be borrowed for two weeks. For a personal retention copy, call Tech. Info. Division, Ext. 5716

LAWRENCE BERKELEY LABORATORY • UNIVERSITY OF CALIFORNIA • BERKELEY

LBL-3114 c.2

DISCLAIMER

This document was prepared as an account of work sponsored by the United States Government. While this document is believed to contain correct information, neither the United States Government nor any agency thereof, nor the Regents of the University of California, nor any of their employees, makes any warranty, express or implied, or assumes any legal responsibility for the accuracy, completeness, or usefulness of any information, apparatus, product, or process disclosed, or represents that its use would not infringe privately owned rights. Reference herein to any specific commercial product, process, or service by its trade name, trademark, manufacturer, or otherwise, does not necessarily constitute or imply its endorsement, recommendation, or favoring by the United States Government or any agency thereof, or the Regents of the University of California. The views and opinions of authors expressed herein do not necessarily state or reflect those of the United States Government or any agency thereof or the Regents of the University of California.

Far-Infrared Generation by Optical Mixing

Y. R. Shen

Department of Physics, University of California
and
Inorganic Materials Research Division,
Lawrence Berkeley Laboratory
Berkeley, California 94720

I. INTRODUCTION

Optical mixing is defined as a process in which two or more optical waves interact and generate new frequency components. It is a nonlinear process which normally occurs in a medium. The direct interaction of waves in free space is too weak to be of any significance.[1] Wave mixing at low frequencies has long been a well-known phenomenon. Modulation, demodulation, and sum- and difference-frequency generation of radio waves and acoustic waves are just a few typical examples. The nonlinear interaction of waves at optical frequencies is often much weaker, and is not easily observable with ordinary light sources. For this reason, the field of optical mixing had not received much attention before the invention of lasers, although demodulation of light in a photodetector may be considered as a well-known example of optical mixing.

By definition, optical mixing includes essentially all the nonlinear optical processes such as sum-frequency generation, parametric process, etc.[2] It would be difficult for us to cover all of them in this review paper. Therefore, we shall limit ourselves here to the case of far-infrared generation by optical mixing only.

The motivation of studying far-infrared generation by optical mixing is twofold. First, the far-infrared generation is closely related to other nonlinear optical processes such as electro-optical effect, sum-frequency generation, etc. By studying the various nonlinear optical processes, we can have a better understanding of not only the nonlinear optical properties of matter, but also optical wave propagation in a nonlinear medium. Second, we hope to find a new far-infrared source which is superior to those presently available. This second aspect is

clearly of practical importance; let us therefore elaborate a little more on it.

The field of far-infrared spectroscopy (particularly in the region between 3 and 200 cm^{-1}) began more than 50 years ago.[3] There is certainly no lack of optical transitions between energy states in this region, e.g., rotational and vibrational levels of molecules, crystal-field-split levels of magnetic ions, phonons, magnons, plasmons, energy gaps in superconductors, etc. Nevertheless, the field has lagged far behind spectroscopy in other parts of the spectrum. The reason is simple. The progress in the field has always been impeded by the lack of bright sources and sensitive detectors.[3] Recently, a great deal of research effort has been devoted to the development of sensitive infrared detectors. For example, Josephson junctions have been developed into a potential far-infrared detector which can be several orders of magnitude more sensitive than the conventional detectors using the bolometer principle.[4] By comparison, only very limited effort has been spent on the development of better far-infrared sources.

The source most commonly used in the infrared is blackbody radiation. A perfect blackbody of surface area 1 cm^2 and temperature 5000K radiates approximately 1000 W over the 4π solid angle, but if we limit the solid angle to 10 milli-sterad and the spectral content to 1 cm^{-1} in the far infrared around 50 cm^{-1}, then the radiated power is only 1.5×10^{-8} W. Electron beam devices, such as klystron, magnetron, carcinotron, etc. have also been used as submillimeter and far-infrared sources up to 25 cm^{-1}; higher frequencies are achievable with the frequency multiplication scheme. However, the efficiency of such devices

falls off very rapidly with increasing frequency. In addition, their tunability is often limited to ± 5%. It is therefore interesting to see whether we can find a better far-infrared source by some novel means.

With the advance of quantum electronics, a number of tunable infrared sources have been developed. Infrared semiconductor lasers cover a spectral range from ~ 300 cm^{-1} to the visible. Spin-flip Raman lasers can tune over a range of about 300 cm^{-1} around 10^3 cm^{-1} with a linewidth of 2×10^{-3} cm^{-1}. Parametric oscillators are useful in the near infrared. In the far infrared, however, the only novel tunable source is obtained by optical mixing in a nonlinear medium. At present, it has already been demonstrated that by using pulsed dye laser beams,[6] one can generate more than 100 mW of far-infrared peak power from a nonlinear crystal. With pulses CO_2 lasers of 200 kW peak power, several hundred mW of far-infrared peak power can be generated.[7,8] Even at the repetition rate of one pulse per second, such a far-infrared source already has an average power higher than any conceivable blackbody source. With higher input laser power and improved mixing geometry, we can now expect even much higher far-infrared output from optical mixing.[8] By using the nonlinear crystal to construct a dielectric waveguide for the far-infrared wave, a conversion efficiency of 20% of the predicted value has been achieved.[9] Far-infrared generation by optical mixing in the cw mode has also become possible. A cw far-infrared power of 10^{-7} W has already been obtained with two 25 W CO_2 laser beams mixed in GaAs.[8] This novel far-infrared source is also tunable over a wide range. With CO_2 lasers as the pump sources, it is not continuously tunable, but has a total of about 3200 lines approximately equally spaced in the range between 5 and 140 cm^{-1}.[7,8] With dye lasers

as the pump sources, it is continuously tunable, in principle, over a range from 0 to ~ 10,000 cm^{-1}, limited only by the absorption bands of the materials.

Tunable far-infrared generation by optical mixing has been seen in a number of very different media. In different cases, the physical mechanisms responsible for optical mixing are different. We shall discuss in the following sections the various cases separately. We also consider the special case of far-infrared generation by optical rectification of ultrashort pulses. The general discussion of far-infrared generation by optical mixing can be applied analogously to the generation of other excitational waves such as acoustic wave, spin wave, etc.

In Section II, we give a brief theoretical description of the problem and point out the inherent computational difficulties of far-infrared generation in the long wavelength limit. Section III covers the experimental observations of far-infrared generation by optical mixing in transparent crystals. Section IV describes how the nonlinear susceptibilities and the far-infrared output vary as the far-infrared frequency approaches an absorption or restrahlung band. The corresponding experimental verification is given. Then, in Section V, we review the theory of far-infrared generation by stimulated polariton scattering together with the available experimental results. In Section VI, we discuss tunable far-infrared generation by optical mixing via a spin

flip transition between two magnetic states. The problem is treated theoretically as a special case of the description in Sections IV and V. We review in Section VII and Section VIII respectively the problems of far-infrared generation by optical mixing in a crystal through optical rectification by absorbing impurities and in metal vapor through resonantly enhanced third-order nonlinearity. We discuss in Section IX the problem of far-infrared generation by optical rectification of picosecond pulses. We then describe briefly in Section X the possibility of generating other excitational waves by optical mixing. Finally, in Section XI, we give a few examples of how optical mixing can be used also as a spectroscopic technique.

Little effort has been spent on the literature search. The author would like to apologize to those whose papers on the subject have been left out of the reference list here.

II. THEORETICAL CONSIDERATION

The basic theory of far-infrared generation by optical mixing is essentially the same as that of sum- and difference-frequency generation.[10] The generation and propagation of the far-infrared field $\vec{E}(\omega)$ is governed by the wave equation

$$[\nabla \times \nabla - \omega^2 \underset{\approx}{\varepsilon}(\omega)/c^2]\vec{E}(\omega) = (4\pi\omega^2/c^2)\vec{P}^{NL}(\omega) \tag{1}$$

where $P^{NL}(\omega)$ is the nonlinear polarization created by the pump fields. For a crystal without inversion symmetry, we have, in the electric-dipole approximation,[2]

$$\vec{P}^{NL}(\omega) \cong \underset{\approx}{\chi}^{(2)}(\omega = \omega_1 - \omega_2) : \vec{E}(\omega_1)\vec{E}^*(\omega_2), \tag{2}$$

and for a medium with inversion symmetry, we have

$$\vec{P}^{NL}(\omega) \cong \underset{\approx}{\chi}^{(3)}(\omega = \omega_1 + \omega_2 - \omega_3) : \vec{E}(\omega_1)\vec{E}(\omega_2)\vec{E}^*(\omega_3) \tag{3}$$

where $\underset{\approx}{\chi}^{(2)}$ and $\underset{\approx}{\chi}^{(3)}$ are second- and third-order nonlinear susceptibility tensors and $\vec{E}(\omega_i)$ are the pump fields at optical frequencies. In this paper, we shall always assume negligible depletion of the pump fields

so that $\vec{P}^{NL}(\omega)$ is known directly from the given input conditions.

The physical picture behind Eq. (1) is that through nonlinear interaction of light with matter, the pump fields set up in the medium an array of oscillating dipoles. These oscillating dipoles are the sources for the far-infrared field $E(\omega)$. The problem is then equivalent to the problem of radiation from an antenna array. It is well known that the rigorous solution of such a problem with appropriate boundary conditions is difficult to obtain. We shall therefore be satisfied with approximate solutions here.

Let us consider first the simplest case where we assume infinite plane waves propagating in a semi-infinite, non-absorbing, isotropic medium with a boundary surface at $z = 0$. With the approximation of a slowly varying amplitude ($|\partial^2 \mathcal{E}(\omega)/\partial z^2| \ll |k_z \partial \mathcal{E}(\omega)/\partial z|$ with the definition $E(\omega) = \mathcal{E}(\omega) \exp(i\vec{k} \cdot \vec{r} - i\omega t)$), Eq. (1) reduces to[2]

$$\frac{\partial \mathcal{E}(\omega)}{\partial z} = \frac{i2\pi\omega^2}{c^2 k_z} P^{NL}(\omega)\, e^{-i\vec{k}\cdot\vec{r}+i\omega t}. \tag{4}$$

If $P^{NL}(\omega) = p^{NL}(\omega) \exp(i\vec{k}_s \cdot \vec{r} - i\omega t)$, then assuming $\mathcal{E}(\omega) = 0$ at $z = 0$, we obtain at $z = \ell$

$$|\mathcal{E}(\omega)|^2 = \left|\frac{2\pi\omega^2}{c^2 k_z} p^{NL}(\omega)\right|^2 \left[\frac{\sin(\Delta k\ell/2)}{(\Delta k\ell/2)}\right]^2 \ell^2 \tag{5}$$

where $\Delta k = k_{sz} - k_z$ is known as the phase mismatch. This is the familiar result one usually obtains for sum- and difference-frequency generation.[2] The output $|\mathcal{E}(\omega)|^2$ is a maximum when $\Delta k = 0$. It yields the maximum energy conversion efficiency as one would expect when both energy

and momentum conservations are satisfied in a nonlinear interaction process.

However, for far-infrared generation, in the long-wavelength limit, the assumption of infinite plane waves may not be a very good approximation. Diffraction effect becomes important when the pump-beam diameter is comparable with the far-infrared wavelength. We should then look for a more general solution of Eq. (1). Let us first assume that a thin slab of the nonlinear medium is immersed in a linear medium with a matching linear refractive index. The far-field solution of Eq. (1) is then given by[11]

$$\vec{E}(\vec{r},\omega) = \left(\frac{\omega}{c}\right)^2 \int_V d^3r' \; (\mathbb{1} - \hat{r}\hat{r}) \cdot \vec{P}^{NL}(\vec{r}',\omega) e^{ik|\vec{r}-\vec{r}'|}/|\vec{r}-\vec{r}'| \qquad (6)$$

where the integration is over the volume V in which the pump fields interact with the nonlinear medium. With $\vec{P}^{NL}(\vec{r}',\omega)$ given, $\vec{E}(\vec{r},\omega)$ can in principle be calculated.

Consider, for example, the pump fields being confined to a cylinder of radius a along $\hat{z}$ such that[5,12]

$$\begin{aligned} \vec{P}^{NL}(\vec{r},\omega) &= \hat{x}\, P^{NL}(\omega) \exp(ik_s z - i\omega t) \qquad &\text{for} \quad (x^2+y^2) \leqslant a^2 \\ &= 0 \qquad &\text{for} \quad (x^2+y^2) > a^2. \end{aligned} \qquad (7)$$

For this case, the integration in Eq. (6) can be performed readily. We are often more interested in the total far-infrared radiated power W collected by a detector. For a detector with a circular area A sitting on the z-axis, we find[12]

$$W = \int_A d^2r |E(\vec{r},\omega)|^2 nc/2\pi$$

$$= \frac{\omega^4 n}{c^3} |P^{NL}(\omega)|^2 \ell^2 (\pi a^2) \int_0^{\theta_m} d\theta \sin\theta \left(\frac{\sin\alpha}{\alpha}\right)^2 \left(\frac{2J_1(\beta)}{\beta}\right)^2 \tag{8}$$

where ℓ is the thickness of the nonlinear thin slab, θ is the angle between $\hat{r}$ and $\hat{z}$, θ_m is the maximum collection angle of the detector, $\alpha = k\ell(1+\Delta k/k-\cos\theta)/2$, $\Delta k = k_s - k$, and $\beta = ka \sin\theta$. The Bessel-function term $[2J_1(\beta)/\beta]^2$ actually describes the effect of diffraction from a circular aperture, and the $(\sin\alpha/\alpha)^2$ term describes the phase-matching condition. If $ka \gg 1$, then $2J_1(\beta)/\beta$ is only appreciable for $\theta < 1/ka$. For such a small θ, we have $\alpha \cong \Delta k\ell/2$. The integral in Eq. (7) with $\theta_m \gg 1/ka$ then yields $(1/k^2a^2) \sin^2(\Delta k\ell/2)/(\Delta k\ell/2)^2$. Equation (8) thus reduces to the same form as one would obtain in the plane wave approximation (see Eq. (5)). This is expected since in the limit of $ka \gg 1$, the diffraction effect should be negligible.

The solution in the form of Eq. (8) is physically transparent, and can be used for order-of-magnitude estimate. However, in obtaining it, we have made several simplifying assumptions. We can of course use a more realistic functional form for $P^{NL}(\vec{r},\omega)$ in Eq. (7), with the result of a more complicated integration to be evaluated. The fact that the nonlinear material is actually immersed in a linear medium (e.g., air) with a very different refractive index is more difficult to cope with in the context of Eq. (6) where the near field and the boundary effects have been neglected. In addition, a far-infrared detector which normally has a tapered light pipe in front of it detects $\int_0^{k_{\perp m}} |\mathcal{E}(\vec{k},\omega)|^2 \, d^2k_\perp$

instead of $\int_A |\mathcal{E}(\vec{r},\omega)|^2 d^2r$, where $\mathcal{E}(\vec{k},\omega)$ is the spatial Fourier component of $\mathcal{E}(\vec{r},\omega)$, and $\vec{k}_\perp$ is perpendicular to the axis of the light pipe. Only if all the far-infrared radiation from the nonlinear medium is collected by the detector, then by the Parseval's theorem, $\int_0^{k_{\perp m}} |\mathcal{E}(\vec{k},\omega)|^2 d^2k_\perp = \int_A |\mathcal{E}(\vec{r},\omega)|^2 d^2r$.

In order to take into account the boundary effects and to calculate W properly, it would be more appropriate to solve for $\mathcal{E}(\vec{k},\omega)$ instead of $\mathcal{E}(\vec{r},\omega)$.[13] Let us write

$$E(\vec{r},\omega) = \int d^2k_\perp \mathcal{E}(\vec{k}_\perp,\omega,z) e^{i(\vec{k}\cdot\vec{r}-\omega t)}$$

$$P^{NL}(\vec{r},\omega) = \int d^2k_\perp p^{NL}(\vec{k}_\perp,\omega,z) e^{i(\vec{k}_s\cdot\vec{r}-\omega t)}. \tag{9}$$

We shall assume here that the field is transverse. Extension to the more general case is quite straightforward. Then, each spatial Fourier component, in the limit of $|\partial^2\mathcal{E}(k)/\partial z^2| \ll |k\partial\mathcal{E}(k)/\partial z|$, obeys the equation

$$\frac{\partial}{\partial z}[\mathcal{E}(\vec{k}_\perp,\omega,z)e^{k''_z z}] = \frac{i2\pi\omega^2}{c^2 k'_z} p^{NL}(\vec{k}_\perp,\omega,z)e^{i\Delta k_z z} \tag{10}$$

where $\Delta k_z = k_{sz} - k_z$ is generally complex; $k_z = k'_z + ik''_z$, and $k''_z = \omega\varepsilon''/2c\sqrt{\varepsilon'}$ is the absorption coefficient. The solution of Eq. (10) at $z = \ell$ is

$$\mathcal{E}(k_\perp,\omega,\ell) = [\mathcal{E}^o + f(\ell)]e^{-k''_z\ell} \tag{11}$$

with

$$f(\ell) = \frac{i2\pi\omega^2}{c^2 k'_z}\int_0^\ell p^{NL}(\vec{k}_\perp,\omega,z)e^{i\Delta k_z z}dz.$$

It is now relatively simple to impose the boundary conditions on each spatial Fourier component. Consider a slab of nonlinear medium with plane boundaries at $z = 0$ and $z = \ell$. Because of reflections at the boundaries, the difference-frequency generation of each Fourier component resolves into four waves

$$\left.\begin{aligned} E_1(\vec{k}_\perp,\omega) &= [\mathcal{E}^o + f(z)]e^{i\vec{k}\cdot\vec{r}-i\omega t} \\ E_2(\vec{k}_\perp,\omega) &= \mathcal{E}_2 e^{i(\vec{k}_\perp - k_z\hat{z})\cdot\vec{r}-i\omega t} \end{aligned}\right\} \text{ for } 0 \leqslant z \leqslant \ell$$

$$E_3(\vec{k}_\perp,\omega) = \mathcal{E}_3 e^{i(\vec{k}_\perp - k_{oz}\hat{z})\cdot\vec{r}-i\omega t} \qquad \text{for } z < 0$$

$$E_4(\vec{k}_\perp,\omega) = \mathcal{E}_4 e^{i(\vec{k}_\perp + k_{oz}\hat{z})\cdot\vec{r}-i\omega t} \qquad \text{for } z > 0 \tag{12}$$

where $k_o = \omega/c$, E_1 and E_4 are forward propagating and E_2 and E_3 are backward propagating. We have assumed that in the crystal, only the E_1 wave can grow steadily with distance as a result of near phase matching in the far-infrared generation. From the conditions imposed on E and H at the boundary surfaces, we can immediately find $\mathcal{E}^o$, $\mathcal{E}_2$, $\mathcal{E}_3$, and $\mathcal{E}_4$ in terms of $f(\ell)$. For example, if the field polarization is perpendicular to the plane of incidence, we obtain for the transmitted wave

$$\mathcal{E}_4 = f(\ell)\ \left[\frac{(1+R)e^{-k''_z\ell}}{1-R^2 e^{i2k_z\ell}}\right] \tag{13}$$

where R is the reflectivity. The term in the square brackets is the Fabry-Perot factor for the resonator formed by the slab boundaries.

We have thus shown that we can find a solution for each spatial

Fourier component of the far-infrared field generated in the crystal with appropriate boundary conditions. The solution depends on $p^{NL}(\vec{k}_\perp,\omega,z)$. Analytical expression of $p^{NL}(\vec{k}_\perp,\omega,z)$ can be obtained if we assume that the pump beams are of single mode (focused or unfocused) with prescribed Gaussian profiles. The calculation is similar to the one used by Bjorkholm[13] and by Kleinman, et al.[14] in obtaining $P^{NL}(\vec{k}_\perp,\omega,z)$ for second harmonic generation. It is tedious but straightforward and hence will not be reproduced here. The reader is referred to Refs. 12-14 for detail. The analytical forms of the solutions are long and complicated. Therefore, it is perhaps more valuable to find the solutions numerically and have the results presented graphically. This is being done and will be published elsewhere.[15] In any case, knowing $\vec{E}(k_\perp,\omega,z)$, we can find $\vec{E}(\vec{r},\omega)$ from Eq. (9) and hence everything we want to know about the far-infrared output.

To conclude this section, we summarize the major physical aspects in which far-infrared generation by optical mixing differs from optical sum-frequency generation. Because of the long wavelength of the far-infrared, diffraction may not be negligible in the far-infrared generation using laser beams of finite cross-sections, and the phase-matching condition can be approximately satisfied over a fairly large cone. Then, the usual infinite-plane-wave approximation is no longer valid. The refractive index of a condensed matter at the far infrared is usually large (~ 5). The boundary effects on the far-infrared generation can be very important. It may happen that because of total reflection, part of the generated far infrared can never get out of the nonlinear medium. Finally, we must also consider the fact that the collection

angle of the detector may be smaller than the cone of far-infrared radiation from the nonlinear medium. These effects of course become more pronounced for longer far-infrared wavelength.

III. EXPERIMENTS ON FAR-INFRARED GENERATION BY OPTICAL MIXING IN A CRYSTAL WITH SECOND-ORDER NONLINEARITY

A large number of experimental reports exists in the literature on difference-frequency generation in a nonlinear crystal by optical mixing of two pump beams. Both near- and far-infrared radiation have been generated by this method. Here, we shall restrict our discussion to submillimeter and far-infrared generation only. A typical experimental setup is shown in Fig. 1.

Zernike and Bermann[16] first reported detection of far-infrared radiation around 100 cm^{-1} resulting from mixing of a large number of modes of a Nd: glass laser pulse in a quartz crystal. The spectral distribution of the far-infrared output in this case was unknown. Later, Zernike[17] also detected far-infrared generation in InSb by mixing of two CO_2 laser lines. The Bell Lab group subsequently reported a number of experiments on far-infrared generation by mixing of CO_2 laser lines in various semiconductors.[18-23] By tuning the CO_2 lines, the frequency of the far-infrared output can be discretely tuned over ~ 200 cm^{-1}. Since the CO_2 laser lines are sharp, the corresponding far-infrared output can have very high spectral purity. The Berkeley group[5] and Yajima and co-workers[24] used two simultaneously Q-switched ruby lasers with different lasing frequencies as the pump sources for far-infrared generation. The formal group emphasized the tunable aspect of the problem and showed that the far-infrared output can be continuously

tuned from 0 to 50 cm^{-1} by tuning the ruby laser frequencies.

More recently, the Berkeley group[6] has succeeded in mixing two pulsed dye-laser beams in nonlinear crystals to generate tunable far-infrared radiation over a wide spectral range. In principle, the tunability can cover a range from 0 to ~ 10,000 cm^{-1}, limited only by the infrared absorption bands of the nonlinear crystals. Both the Berkeley group[6] and the National Magnet Lab group[7,8] have demonstrated that far-infrared generation by optical mixing with non-collinear phase matching can be efficient. Using the multiple total-reflection scheme first suggested by Armstrong _et al_,[10] and using two CO_2 lasers (25 W) as pump sources, the National Magnet Lab group has actually been able to generate cw far-infrared output of 10^{-7} W (discretely tunable) from a GaAs crystal.[8] With a thin slab of GaAs forming a waveguide for the generated far infrared, Thompson and Coleman[9] have observed a maximum conversion efficiency of 20% of the predicted value.

Tunable far-infrared radiation can also be generated by stimulated polariton scattering,[25,26] by spin-flip Raman transitions,[27] and by third-order wave mixing in gases.[28] These cases will be discussed separately in more detail in later sections. Here, we shall consider only far-infrared generation by optical mixing of two pump beams in a more or less transparent nonlinear crystal.

For the second-order nonlinear processes, the nonlinear polarization is given by Eq. (2). The corresponding nonlinear susceptibility $\chi^{(2)}$ has the permutation symmetry[2]

$$\chi^{(2)}_{\ell mn}\ (\omega_1 = \omega_2+\omega) = \chi^{(2)}_{mn\ell}\ (\omega_2 = -\omega+\omega_1) = \chi^{(2)}_{n\ell m}\ (\omega = \omega_1-\omega_2) \qquad (14)$$

when absorption is negligible. If the electro-optical coefficient $r_{\ell mn} = [4\pi/\varepsilon(\omega_1)\varepsilon(\omega_2)]\ \chi^{(2)}_{\ell mn}\ (\omega_1 = \omega_2+\omega)|_{\omega\to 0}$ is known, then we can immediately obtain an estimate of $\chi^{(2)}_{n\ell m}(\omega = \omega_1-\omega_2)$ from Eq. (14), although the estimated value of $\chi^{(2)}_{n\ell m}(\omega = \omega_1-\omega_2)$ may be somewhat different from the real value because of dispersion and absorption. Knowing $\chi^{(2)}_{n\ell m}(\omega = \omega_1-\omega_2)$, we can then have a quick estimate of the far-infrared output using, say, Eq. (8). For example, we find for $LiNbO_3$,[5,29] $\chi^{(2)}_{yyy}(\omega = \omega_1-\omega_2)|_{\omega\to 0} = 4.5 \times 10^{-8}$ esu for $\omega_1 \cong \omega_2$ at the ruby laser frequencies. We then calculate from Eq. (8) that with two ruby laser beams of 1 MW each over an area of 0.2 cm^2, a far-infrared power of about 3 mW at 10 cm^{-1} can be generated from a crystal of 0.05 cm thick under the phase matching condition. Experimentally, 1 mW at 8.1 cm^{-1} from a 0.047 cm $LiNbO_3$ crystal was detected.[5] The lasers used in the experiments did not have simple spatial mode structure. This makes the more rigorous theoretical estimate quite difficult. Similar order-of-magnitude agreement between theory and experiment in the far-infrared output has been found in the mixing experiments using CO_2 lasers.[7,8,18-23]

As one would expect, the efficiency of far-infrared generation by optical mixing depends critically on the phase mismatch. Most of the experiments were designed to study the possibility of achieving phase matching. In anisotropic crystals, collinear phase matching for both forward and backward far-infrared generation can be realized by using the birefringent property of the crystal.[5,22] In cubic crystals, however, collinear phase matching can only be achieved with the help of anomalous dispersion of refractive indices,[17,20] or the magneto-optical effect of free carriers.[19] It turns out that, because of the small wave vector of

the far infrared, the forward collinear phase mismatch $\Delta k = |k_1 - k_2 - k| < k$ is usually small even in the non-matched cases. In other words, the coherent length for the far-infrared generation can be fairly large ($\gtrsim$ 1 mm at 10 cm^{-1}). It may be comparable to the effective length of the crystal when there is strong far-infrared absorption. In most nonlinear crystals, non-collinear phase matching can always be achieved over a limited frequency range.

So far, very few experiments have been designed to study the characteristics of the far-infrared output. Thus, the Berkeley group is the only group who has carefully analyzed the spectrum of the output.[5] They have tried to look for the effects of absorption, diffraction, walk-off due to double refraction, etc., by comparing the far-infrared output from crystals of different lengths. They have also tried to measure the effects of the crystal boundaries and the angular distribution of the outgoing far-infrared radiation.[5,12] However, the experiments have not been very successful because of the inherent difficulties in achieving high accuracy in the far-infrared measurements and because of the poor mode structure of the lasers used in the experiments. We believe that in the future, such experiments should be performed with single-mode CO_2 lasers.

Several research workers have investigated the far-infrared generation near a far-infrared resonant absorption line or band.[23,30] While the nonlinear susceptibility $\chi^{(2)}$ increases because of resonant enhancement, the linear absorption also increases correspondingly. Therefore, the increase or decrease of the far-infrared output is the result of competition between the resonant behavior of $\chi^{(2)}$ and of the linear

absorption. This is an interesting problem. We shall therefore have a more thorough discussion on it in the following section.

IV. FAR-INFRARED GENERATION BY OPTICAL MIXING NEAR A POLARITON MODE IN A NONLINEAR CRYSTAL

Near a far-infrared absorption line, the nonlinear susceptibility $\chi^{(2)}(\omega = \omega_1 - \omega_2)$ can be decomposed into two parts

$$\chi^{(2)}(\omega) = \chi_\infty^{(2)}(\omega) + \chi_L^{(2)}(\omega)$$

where $\chi_L^{(2)}(\omega)$ is the contribution from the material excitation responsible for the far-infrared absorption, and $\chi_\infty^{(2)}$ is the non-resonant contribution. Physically, $\chi_L^{(2)}(\omega = \omega_1 - \omega_2)$ exists because the pump fields $E(\omega_1)$ and $E(\omega_2)$ couple nonlinearly with the material excitation while the far-infrared field $E(\omega)$ couples linearly with it. We can derive explicitly the expression of $\chi_L^{(2)}$ in terms of the coupling coefficients.

Let us assume, for example, the material excitation to be an optical phonon wave $Q(\omega)$. The reader should bear in mind that the derivation here applies analogously to other material excitations such as magnons, plasmons, etc. Generalization to a set of excitational modes is also straightforward. The mixing of the two pump fields now generate not only $E(\omega)$ but also $Q(\omega)$. In addition, $E(\omega)$ and $Q(\omega)$ interact linearly. Therefore, the wave equations for the four coupled waves are

$$[\nabla x \nabla x - \omega_1^2 \underset{\approx}{\varepsilon}(\omega_1)/c^2]\, \vec{E}(\omega_1) = (4\pi\omega_1^2/c^2)[\underset{\approx}{\chi}_\infty^{(2)} \vec{E}(\omega_2)\vec{E}(\omega) + \underset{\approx}{f}^* : \vec{E}(\omega_2)\vec{Q}(\omega)] \tag{15a}$$

$$[\nabla x \nabla x - \omega_2^2 \underset{\approx}{\varepsilon}(\omega_2)/c^2]\vec{E}(\omega_2) = (4\pi\omega_2^2/c^2)[\underset{\approx}{\chi}_\infty^{(2)} : \vec{E}(\omega_1)\vec{E}^*(\omega) + \underset{\approx}{f} : \vec{E}(\omega_1)Q^*(\omega)] \tag{15b}$$

$$[\nabla x \nabla x - \omega^2 \underset{\approx}{\varepsilon}_\infty(\omega)/c^2]\vec{E}(\omega) = (4\pi\omega^2/c^2)[\underset{\approx}{A} \cdot \vec{Q} + \underset{\approx}{\chi}_\infty^{(2)} : \vec{E}(\omega_1)\vec{E}^*(\omega_2)] \tag{15c}$$

$$(\omega_o^2 - \omega^2 - i\omega\Gamma)\vec{Q} = \underset{\approx}{A} \cdot \vec{E}(\omega) + \underset{\approx}{f} : \vec{E}(\omega_1)\vec{E}^*(\omega_2) \tag{15d}$$

where $\underset{\approx}{\varepsilon}_\infty(\omega)$ is the non-resonant part of the linear dielectric constant and ω_o is the resonant frequency of $\vec{Q}$. The linear and nonlinear coupling coefficients are $\underset{\approx}{A}$ and $\underset{\approx}{f} = \partial\underset{\approx}{\varepsilon}/\partial\vec{Q}$ respectively, both taken to be real. The microscopic expressions for $\underset{\approx}{\chi}_\infty$, $\underset{\approx}{f}$ and $\underset{\approx}{A}$ can easily be derived, as have been done in the literature.[10,31] Both $\underset{\approx}{\chi}_\infty^{(2)}$ and $\underset{\approx}{f}$ will show resonant enhancement if ω_1 or ω_2 approach an electronic absorption band, but has practically no change if the difference frequency ω varies around ω_o. The coefficient $\underset{\approx}{A}$ which is proportional to the matrix element of the far-infrared absorption should generally show little or no dispersion.

Eliminating $\vec{Q}$ from Eqs. (15c) and (15d), we find

$$[\nabla x \nabla x - \omega^2 \underset{\approx}{\varepsilon}(\omega)/c^2]\vec{E}(\omega) = (4\pi\omega^2/c^2)\, \underset{\approx}{\chi}^{(2)}(\omega = \omega_1 - \omega_2) : E(\omega_1)E^*(\omega_2) \tag{16}$$

where

$$\underset{\approx}{\varepsilon}(\omega) = \underset{\approx}{\varepsilon}_{\infty}(\omega) + 4\pi\underset{\approx}{\chi}_L^{(1)}(\omega) \tag{17}$$

with $$\underset{\approx}{\chi}_L^{(1)}(\omega) = \underset{\approx}{A} : \underset{\approx}{A}/(\omega_o^2 - \omega^2 - i\omega\Gamma)$$

$$\underset{\approx}{\chi}^{(2)}(\omega = \omega_1 - \omega_2) = \underset{\approx}{\chi}_{\infty}^{(2)} + \underset{\approx}{\chi}_L^{(2)}(\omega) \tag{18}$$

with $$\underset{\approx}{\chi}_L^{(2)}(\omega) = \underset{\approx}{A} : \underset{\approx}{f}/(\omega_o^2 - \omega^2 - i\omega\Gamma).$$

Note that $k = (\omega/c)\varepsilon^{1/2}(\omega)$, plotted in Fig. 2, is the dispersion relation of the so-called polariton mode,[32] which results from linear coupling of $E(\omega)$ and $Q(\omega)$. We can also find, from Eqs. (15b) and (15d),

$$\{\nabla x \nabla x - (\omega_2/c)^2[\varepsilon(\omega_2) + 4\pi\, \underset{\approx}{\chi}_R^{(3)} : \vec{E}(\omega_1)\vec{E}^*(\omega_1)]\} \cdot \vec{E}(\omega_2)$$

$$= (4\pi\omega_2^2/c^2)\underset{\approx}{\chi}^{(2)}(\omega)^* : \vec{E}(\omega_1)\vec{E}^*(\omega_2) \tag{19}$$

where

$$\underset{\approx}{\chi}_R^{(3)} = \underset{\approx}{f} \cdot \underset{\approx}{f}/(\omega_o^2 - \omega^2 + i\omega\Gamma)$$

is known as the Raman susceptibility.[31] We then have the simple relation[33]

$$\chi_L^{(2)} = [\chi_L^{(1)}\ \chi_R^{(3)*}]^{1/2}. \tag{20}$$

Note, however, that Eq. (20) is only true when only one mode dominates the resonant absorption.

In general, we can deduce $\chi_L^{(1)}(\omega)$ and $\chi_R^{(3)}$, and hence A and f, from linear absorption and Raman scattering measurements respectively. We can then obtain $\chi_L^{(2)}$ from Eq. (18). Knowing $\chi_L^{(2)}$ and the electro-optical coefficient $r_{\ell mn}$, we can also find $\chi_\infty^{(2)}$ from the relation

$$\chi^{(2)}_{n\ell m}(\omega=\omega_1-\omega_2)_{\omega\to 0} = \varepsilon_\ell(\omega_1)\varepsilon_m(\omega_2)r_{\ell mn}/4\pi$$

$$= [\chi_\infty^{(2)}+\chi_L^{(2)}]_{n\ell m}(\omega=\omega_1-\omega_2)_{\omega\to 0}. \tag{21}$$

In some cases, $\underset{\approx}{\chi}_\infty^{(2)}$ can also be estimated from the results of second-harmonic generation if the dispersion in $\underset{\approx}{\chi}_\infty^{(2)}$ can be neglected. An example of $\chi^{(2)}(\omega)$ vs ω is shown in Fig. 3.

Let us now consider how the resonant enhancement in $\underset{\approx}{\chi}^{(2)}(\omega)$ and in $\underset{\approx}{\varepsilon}(\omega)$ affect the far-infrared output as governed by Eq. (16). For this purpose, we can use the plane-wave approximation which reduces Eq. (16) to the form of Eq. (10). The solution is

$$|E(\omega,\ell)|^2 = \left(\frac{2\pi\omega^2}{c^2k'_z}\right)^2|E(\omega_1)|^2|E(\omega_2)|^2\, F(\ell) \tag{22}$$

where

$$F(\ell) = \frac{|\chi^{(2)}|^2}{(\Delta k'_z)^2+(\Delta k''_z)^2}\,|e^{i\Delta k_z\ell}-1|^2 e^{-2k''_z\ell} \tag{23}$$

$$\Delta k_z = \Delta k'_z + i\Delta k''_z$$

$$\Delta k'_z = k'_{1z}-k'_{2z}-k'_z$$

$$\Delta k''_z = k''_{1z}+k''_{2z}-k''_z, \qquad k''_z = \omega^2\varepsilon''/2c^2k'_z\,.$$

At phase matching $\Delta k'_z = 0$, we have

$$F(\ell) = [|\chi^{(2)}|^2/(\Delta k''_z)^2]|e^{-\Delta k''_z \ell}-1|^2 e^{-2k''_z \ell} \tag{24}$$

when either ω_1 or ω_2 or ω approaches resonance, both $|\chi^{(2)}|$ and Δk_z show a resonant effect. Then, as seen from Eq. (23), it is not <u>à priori</u> clear whether $|E(\omega)|^2$ would increase or decrease.

We shall consider the case where the far-infrared frequency ω approaches a polariton resonance mode. De Martini[30] has studied the problem of far-infrared generation by optical mixing near a polariton mode in a cubic crystal in great detail both experimentally and theoretically. We shall discuss only the qualitative features here.

Let us discuss the problem of phase matching first. In order to achieve phase matching, collinear or noncollinear, we must have

$$|k'_1(\omega_1) - k'_2(\omega_2)| \leqslant |k'(\omega)| \leqslant |k'_1(\omega_1) + k'_2(\omega_1)|.$$

The equality signs apply for collinear phase matching. In a cubic crystal, noncollinear phase matching is always possible as long as the refractive indices have the inequality $n'(\omega) > n'(\omega_1), n'(\omega_2)$. With ω in the vicinity of a lattice mode, this is generally true for $\omega < \omega_o$ only. In addition, collinear phase matching can be realized in a cubic crystal only with the help of anomalous dispersion.

The same general argument applies to noncubic crystals except that collinear phase matching can now be achieved with the help of optical birefringence. Thus, there is a range of ω within which we can obtain collinear phase matching for given ω and ω_1 simply by rotating the crystal.

Assume that we can always satisfy the phase-matching condition or

we can have the coherent length $1/|\Delta k_z|$ longer than the crystal length for $\omega < \omega_o$. How would the far-infrared output power vary as ω approaches ω_o? From Eq. (23) or (24), we have, for $\Delta k'_z = 0$ and $\Delta k''_z = -k''_z$,

$$F(\ell) = [|\chi^{(2)}|^2/k''_z{}^2]|1-e^{-k''_z\ell}|^2. \tag{25}$$

We therefore expect to find the output $|E(\omega)|^2$ to be proportional to $|\chi^{(2)}(\omega)|^2\ell^2$ as long as $k''_z\ell \ll 1$. Increase or decrease of $|\chi^{(2)}(\omega)|$ as ω approaches ω_o depends on whether the two terms of $|\chi^{(2)}(\omega)|$ in Eq. (18) interfere constructively or destructively. We show in Fig. 3 the resonant behavior of $|\chi^{(2)}(\omega)|$ near the 366 cm^{-1} lattice mode of GaP as an example.[34] In this case, the two terms of $|\chi^{(2)}(\omega)|$ have opposite signs for $\omega < \omega_o$. In Fig. 4, for the 248 cm^{-1} lattice mode of $LiNbO_3$, $|\chi^{(2)}(\omega)|$ increases as ω approaches ω_o because the two terms in $|\chi^{(2)}(\omega)|$ interfere constructively for $\omega < \omega_o$.[35] When ω gets sufficiently close to ω_o, the output $|E(\omega)|^2$ should drop rapidly according to Eq. (23) as the far-infrared absorption increases. (For example, the absorption coefficient of GaP for ω around ω_o is shown in Fig. 7.) Immediately above ω_o, the far-infrared output should be very weak not only because of the strong far-infrared absorption but also because of the large phase mismatch.

DeMartini[30] has carried out measurements on the dispersive effect of the far-infrared output in GaP. His results are reproduced here in Fig. 5. For a better comparison with theory, the measurements should be repeated with more data points. Yang et al.[6] have studied the dispersion of the far-infrared output in $LiNbO_3$ with both collinear and

noncollinear phase matching. Their experimental results shown in Fig. 6 are in fairly good agreement with the theoretical calculation.

It is possible that in some cases, the infrared oscillator strength of the material excitation mode is weak so that the linear propagation characteristics of the far-infrared is dominated by $\varepsilon_\infty(\omega)$ rather than by $\chi_L^{(1)}(\omega)$, even when $\omega \approx \omega_o$. Then, as ω varies around ω_o, $\varepsilon_\infty(\omega)$ essentially remains unchanged, and hence the far-infrared output $|E(\omega)|^2$ is proportional to $|\chi^{(2)}(\omega)|^2$. However, in $\chi_\infty^{(2)}(\omega)$, the resonant behavior of $\chi_L^{(2)}(\omega)$ can still dominate over $\chi_\infty^{(2)}(\omega)$. This is true when the mode is strongly Raman active. As a result, the far-infrared output can appear with a strong resonant enhancement at $\omega \approx \omega_o$. We shall give in Section VI a practical example of such a case.

V. FAR-INFRARED GENERATION BY STIMULATED POLARITON SCATTERING

It is also possible to generate tunable far-infrared radiation through stimulated Raman scattering by polaritons, i.e., a composite mode of infrared and material excitational waves.[32] In that case, $E(\omega_1)$ is the only pump field. If it is above a certain threshold, then the Stokes field $E(\omega_2)$, the infrared field $E(\omega)$, and the material excitational wave $Q(\omega)$ can all be generated through amplification of noise. As we would expect, the threshold is nearly a minimum when the phase-matching condition of this nonlinear process is more or less satisfied. Tunability can be achieved by varying the relative propagation directions of $E(\omega_1)$ and $E(\omega_2)$ in order to satisfy the phase-matching condition for a pre-selected polariton mode on the dispersion curve of Fig. 2.

The theory of stimulated polariton scattering has been worked out by many authors.[36-40] It is governed by the same set of equations in Eq. (15). Here, we shall concentrate on the problem of far-infrared generation. We assume that the pump field $E(\omega_1)$ is not attenuated or depleted in the process. Then, by eliminating $Q(\omega)$ in Eqs. (15b-d), we obtain Eqs. (16) and (19) which describe fully the stimulated polariton scattering process. They are now in the same form as the set of equations describing parametric amplification or oscillation.[2] Therefore, the solution is well known. We have

$$E^*(\omega_2) = [\mathcal{E}_+^*(\omega_2)\ \exp(i\Delta K_+ z) + \mathcal{E}_-^*(\omega_2)\ \exp(i\Delta K_- z)]\ \exp(-i\vec{k}_2'\cdot\vec{r})$$

$$E(\omega_3) = [\mathcal{E}_+(\omega_3)\ \exp(i\Delta K_+ z) + \mathcal{E}_-(\omega_3)\ \exp(i\Delta K_- z)]\ \exp(i\vec{k}'\cdot\vec{r}+i\Delta k_z z) \tag{26}$$

where

$$\vec{k} = \vec{k}' + i\vec{k}''$$

$$k' = (\omega/c)\ (\varepsilon')^{1/2}, \qquad k'' = (\omega/c)\ (\varepsilon''/2\sqrt{\varepsilon'})$$

$$\Delta k_z = k_{1z}' - k_{2z}' - k_z'$$

$$\Delta K_\pm = 1/2\{(\gamma_2-\gamma) \pm [(\gamma_2+\gamma)^2 - 4\Lambda]^{1/2}\}$$

$$\gamma_2 = (k_2'/k_{2z}')\ (ik_2'' + k_R)$$

$$k_R = (\omega_2{}^2/2k_{2z}'c^2)\ 4\pi\chi_R|E(\omega_1)|^2$$

$$\gamma = -\Delta k_z - i(k'/k_z')k''$$

$$\Lambda = (4\pi^2\omega_2{}^2\omega^2/c^2k_{2z}'k_z')\ (\chi^{(2)})^2|E(\omega_1)|^2$$

$$|\mathcal{E}(\omega_3)/\mathcal{E}^*(\omega_2)|_\pm = (\omega^2k_{2z}'/\omega_2{}^2k_z')^{1/2}|\Lambda^{1/2}/(\Delta K_\pm + \gamma)|. \tag{27}$$

The exponential gain of the fields along $\hat{z}$ is given by

$$g_{\pm} = - \mathrm{Im}(\Delta K_{\pm}). \tag{28}$$

It is seen that both g and $|\mathcal{E}/\mathcal{E}_2|$ depend critically on the relative values of γ_2, γ, and Λ. Two limits are of interest.[38] First, when $|\gamma+\gamma_2|^2 \gg 4\Lambda$, we have $g_+ \cong - \mathrm{Im}\ \gamma_2$ which is positive if $\varepsilon_2'' < \mathrm{Im}\ (4\pi\chi_R|E_1|^2)$. The corresponding ratio $|\mathcal{E}(\omega)/\mathcal{E}^*(\omega_2)|$ according to Eq. (27) is extremely small. This happens when ω approaches the resonance frequency ω_o of the lattice mode and the coupling between $E(\omega)$ and $Q(\omega)$ becomes very weak so that the polariton wave is essentially all of phonon character. What we then have is actually the usual stimulated Raman scattering by phonons with the far-infrared wave essentially unexcited. Second, when ω is sufficiently far away from ω_o so that $4\pi\chi_R|E_1|^2$ in γ_2 is negligibly small, the stimulated gain g reduces to that of a parametric down-converter.[2] The gain is positive near phase matching and is maximum at phase matching. The ratio $|\mathcal{E}(\omega)/\mathcal{E}^*(\omega_2)|$ is large. This happens when the polariton wave is essentially all of photon character. In general, away from the two limits, how the gain g and the ratio $|\mathcal{E}(\omega)/\mathcal{E}^*(\omega_2)|$ vary depends on the variations of $\varepsilon(\omega)$, χ_R, and $\chi^{(2)}$ with ω.

Henry and Garrett[39] have calculated g_{max} and the corresponding $|\mathcal{E}(\omega)/\mathcal{E}^*(\omega_2)|^2$ as a function of ω for GaP around the 366 cm^{-1} lattice mode. (Phase matching cannot be achieved for the upper branch of the polariton dispersion curve in this case.) Their results are shown in Fig. 7. Here, the terms of $\chi^{(2)}$ in Eq. (18) have opposite signs for

$\omega < \omega_o$. Sussman[35] has made similar calculation for the 248 cm^{-1} mode of $LiNbO_3$. His results are shown in Fig. 8. The two terms of $\chi^{(2)}$ now have constructive interference for $\omega < \omega_o$. Consequently, the curves in Fig. 8 are quite different from those in Fig. 7.

Experimentally, stimulated polariton scattering has been observed by several research groups.[25,26,41] By adjusting the relative angle between $\vec{k}_1$ and $\vec{k}_2$ to achieve phase matching for a given set of frequencies ω, ω_1, and ω_2, tunable far-infrared radiation can be generated. Using a 1-MW Q-switched ruby laser beam of about 2-mm in diameter and a 50-cm focal-length lens to focus the beam into a 3.3 cm a-axis $LiNbO_3$ crystal, Yarborough et al.[25] have detected a far-infrared output with a peak power of 5 W, tunable from 50 cm^{-1} to 200 cm^{-1}. Unfortunately, the threshold for stimulated polariton scattering is quite close to the damage threshold in $LiNbO_3$. A good single-mode laser must be used as the pump source in order to avoid increase of damage probability by inhomogeneity in the beam.

VI. FAR-INFRARED GENERATION BY OPTICAL MIXING VIA A SPIN-FLIP TRANSITION

We have mentioned that in general a polariton is defined as a composite mode of infrared and material excitational waves. Thus, for example, the material excitation can also be an electronic excitation. In particular, it can be a spin-flip excitation between two Zeeman-split magnetic levels. We therefore expect that far-infrared radiation can be generated at frequencies in the vicinity of the spin-flip transition frequency and tunability can be achieved by varying the Zeeman splitting.

What we need is a dynamic equation of motion for the electronic excitational wave to replace the phonon wave equation in the earlier discussion. This turns out to be the Schrödinger's wave equation for the perturbed excited state.[42] We can take $\psi(\omega) = \langle f|g_o\rangle$ as the excitational wave where $\langle f|$ is the perturbed excited state and $\langle g_o|$ is the unperturbed ground state. The corresponding wave equation is[42]

$$\hbar(i\frac{\partial}{\partial t} - \omega_o + i\Gamma)\psi(\omega) = S^{(1)}\, E(\omega_3) + S^{(2)}\, E(\omega_1)E^*(\omega_2) \tag{29}$$

where $S^{(1)}$ and $S^{(2)}$, obtained from first- and second-order perturbations respectively, are related to the linear and Raman susceptibilities. (For simplicity, we consider $S^{(1)}$ and $S^{(2)}$ as scalars.)

$$\chi_L^{(1)} = -\,|S^{(1)}|^2/\hbar(\omega-\omega_o+i\Gamma)$$

$$\chi_R^{(3)} = -\,|S^{(2)}|^2/\hbar(\omega-\omega_o-i\Gamma) \tag{30}$$

which can be measured experimentally.

Equation (29) now replaces Eq. (15c) in the set of coupled equations with Q replaced by $(\hbar/2\omega)^{1/2}\,\dot{\psi}$, A by $-(2\omega/\hbar)^{1/2}\,S^{(1)}$, and f by $-(2\omega/\hbar)^{1/2}\,S^{(2)}$. Then, by eliminating ψ in the set of coupled equations, we again find Eqs. (16) and (19) with

$$\varepsilon(\omega) = \varepsilon_\infty + 4\pi\chi_L^{(1)}(\omega)$$

$$\chi^{(2)}(\omega) = \chi_\infty^{(2)}(\omega) + \chi_L^{(2)}(\omega)$$

$$\chi_L^{(2)}(\omega) = -S^{(1)}S^{(2)}/(\omega-\omega_o+i\Gamma) = (\chi^{(2)}\chi_R^{(3)*})^{1/2} \quad . \tag{31}$$

(More rigorously, we have to take into account the thermal populations in both states at finite temperatures. This can be done by simply incorporating the population difference $(\rho_g-\rho_f)$ as a multiplication factor in the expressions of $\chi_L^{(1)}$, $\chi_L^{(2)}$, and $\chi_R^{(3)}$.) The solution is again in the form of Eq. (2) for far-infrared generation by optical mixing and in the form of Eqs. (26-28) for far-infrared generation by stimulated polariton scattering. The general discussion in the previous sections also applies here.

We now consider a more special case where the electronic excitation is forbidden by electric-dipole transitions, but allowed by magnetic-dipole transitions as in the case of spin-flip transitions. Then, the coupling coefficient $S^{(1)}$ is very small, and consequently, the polariton dispersion curve in Fig. 2 has a very small gap. However, the coefficient $S^{(2)}$ can still be large if the Raman cross-section for this excitation is large. This is the case for the spin-flip transitions between Landau levels in InSb. Both the infrared absorption and the Raman cross-section for such a transition in InSb have been measured. In addition, ε_∞ and $\chi_\infty^{(2)}$ are known. Hence, the functions $\varepsilon(\omega)$, $\chi^{(2)}(\omega)$, and $\chi_R^{(3)}(\omega)$ can all be calculated.[27,43]

Consider first far-infrared generation by optical mixing near the spin-flip transition in InSb, as has been observed by Nguyen and Bridges.[27] In this case, since the magnetic-dipole oscillator strength is weak, the

phase mismatch $\Delta k'_z$ and the attenuation constants k''_z in Eq. (23) do not vary appreciably as ω sweeps across the spin resonance line. The far-infrared output is therefore proportional to $|\chi^{(2)}(\omega)|^2$ which shows a sharp resonant enhancement according to Eq. (31). This was actually demonstrated experimentally by Nguyen and Bridges.[27] Their results are in very good agreement with theoretical calculation as shown in Fig. 9. In their experiment, two collinear CO_2 laser beams were used. The estimated far-infrared output intensity from a 0.4 cm crystal is 1.6×10^{-14} W/cm^2 with the pump intensities at 1 W/cm^2. This output intensity should increase if the phase mismatch $\Delta k'_z$ is reduced. The far-infrared frequency can be tuned over a wide range by varying the relative frequencies of the pump beams in steps with the Zeeman splitting controlled by an external magnetic field.[27]

Consider next far-infrared generation by stimulated polariton or spin-flip Raman scattering in InSb. The solution given by Eqs. (26-28) is plotted in Fig. 10. Since the coupling between the infrared wave and the magnetic excitation is weak, the stimulated gain is essentially just the stimulated Raman gain $g = -\,\mathrm{Im}\chi_R^{(3)}$. In the collinear case, the phase mismatch is large and hence, excitation of the infrared wave is weak, or the ratio $|E(\omega)/E(\omega_2)^*|$ is small. This ratio can become appreciably larger if we allow the beams to be noncollinear in order to achieve phase matching, as shown in Fig. 10. Although stimulated spin-flip Raman scattering has been observed and well studied as a potential tunable source,[44] no far-infrared radiation has yet been detected in the process. However, so far, only the collinear phase-nonmatching case has been tried.[27]

Again, we should emphasize that the above discussion applies generally to any electronic excitation, such as magnons, and impurity levels in solids, electronic levels in gases, etc. All these cases have not yet been explored.

VII. FAR-INFRARED GENERATION BY OPTICAL MIXING THROUGH OPTICAL EXCITATION OF ABSORBING DEFECTS OR IMPURITIES

We recall that in the optical mixing process, the nonlinear polarization $\vec{P}^{NL}(\omega)$ is the source of the far-infrared field (see Eq. (1)). For a crystal without inversion symmetry, we have

$$\vec{P}^{NL}(\omega) = \chi^{(2)}(\omega=\omega_1-\omega_2)E(\omega_1)E^*(\omega_2).$$

In the usual studies of far-infrared generation by optical mixing, we deal with crystals which are transperent to the pump fields. The nonlinear suspectibility $\chi^{(2)}(\omega)$ is an intrinsic property of the pure crystal. It comes from both pure electronic contribution and contribution from coupling of em fields to the infrared-active material excitations. However, a large nonlinear polarization can also be created by optical mixing in an acentric polar crystal through defect or impurity absorption.[45-48]

Two physical mechanisms are responsible for the nonlinear polarization created by impurity (or defect) absorption.[45] First, an impurity polarized in the acentric polar host lattice may have a different dipole moment in the excited state than in the ground state. This may lead to a net polarization when the impurities are excited by the pump field.

Second, nonradiative relaxation of the excited impurities increases the temperature of the host lattice, and a net polarization is then induced via the pyroelectric effect. For the linear absorption, the approximate equation which governs the time variation of the nonlinear polarization induced by these two effects is[45]

$$\left(\frac{\partial}{\partial t} + \frac{1}{\tau}\right) P^{NL}_{(t)} = \frac{\alpha(\Delta\mu)I(t)}{\hbar\omega_1} + \frac{1}{\tau}\left[\frac{p}{C_V}\alpha\int_{-\infty}^{t} I(t)dt\right] \tag{32}$$

where τ is the nonradiative relaxation time of the excited state of the impurities, α is the absorption coefficient, $\Delta\mu$ is the average dipole moment induced per impurity when the impurities are excited to the excited state, p is the pyroelectric coefficient, C_V is the specific heat, and $I(t) = c|E(t)|^2/2\pi$ is the incident light intensity. Note that, in the presence of two monochromatic pump fields, we have $E(t) = E(\omega_1) + E(\omega_2)$.

We can solve Eq. (32) for a particular Fourier component $P^{NL}(\omega=\omega_1-\omega_2)$ induced by $I(\omega) = cE(\omega_1)E^*(\omega_2)/2\pi$. We find

$$\chi^{(2)}_{(\omega)} = \frac{c\alpha(\Delta\mu)\tau}{2\pi\hbar\omega_1(1-i\omega\tau)} + \frac{icp\alpha}{2\pi C_V\omega(1-i\omega\tau)} \tag{33}$$

where the first term is due to the induced dipolar effect, and the second term is due to the pyroelectric effect. It is seen that $\chi^{(2)}(\omega)$ is proportional to α, and hence the far-infrared generation by these effects should be stronger for stronger impurity absorption. As seen from Eq. (33), $\chi^{(2)}(\omega)$ has a cutoff frequency at $\omega\tau \sim 1$. The relaxation time τ depends on both the impurities and the host lattice. For example, the $^2T_2$ state of Cu^{++} in $LiTaO_3$ has τ = 30 psec and the state of Cr^{3+} in

$LiTaO_3$ has τ =2μsec at 300K.

Auston et al.[45] first suggested such a mechanism for far-infrared generation by optical mixing. They have also performed detailed experimental study on the process in a number of different crystals, and shown that the efficiency of far-infrared generation at low frequency (1- 30 cm^{-1}) is quite high. For example, a reduced black $LiNbO_3$ with an absorption coefficient of 200 cm^{-1} at the pump frequency can generate 4 times more far-infrared power at 10 cm^{-1} than a 0.9 mm unreduced $LiNbO_3$.[48]

Far-infrared generation by impurity absorption has the advantage that it eliminates the need of phase matching since we can increase $\chi^{(2)}(\omega)$ by increasing impurity absorption and accordingly reduce the effective crystal length to less than the coherent length. However, this is also the disadvantage since then the maximum far-infrared output is limited by the effective crystal length. The nonlinear polarization P(t) can also be detected as a current pulse in the crystal with the proper electric circuit.[46] This can be used to construct fast pyroelectric detectors if the crystals have short enough τ.

VIII. FAR-INFRARED GENERATION BY OPTICAL MIXING IN VAPOR

In a medium with inversion symmetry, the second-order nonlinear susceptibility $\chi^{(2)}$ is zero in the electric-dipole approximation. The third-order nonlinear susceptibility $\chi^{(3)}$ is usually also small. However, $\chi^{(3)}$ can become very large through resonant enhancement.[49,50] When this happens, the third-order nonlinear optical processes become easily detectable, even in low-pressure gases. Observations of both ultraviolet[51,52] and infrared generation[50] by third-order optical mixing have been reported.

Here, we shall consider far-infrared generation in alkali vapor only.

In Fig. 11, we show the energy level diagram of potassium. We expect the creation of a nonlinear polarization $P^{NL}(\omega) = \chi^{(3)}(\omega=\omega_1-\omega_2-\omega_3)E(\omega_1)E^*(\omega_2)E^*(\omega_3)$ at the infrared frequency ω by the three pump fields $E(\omega_1)$, $E(\omega_2)$, and $E(\omega_3)$. Let ω_1 and ω_2 be close to the resonant frequencies of $4s \rightarrow 5p$ and $5s \rightarrow 5p$ respectively. Then, $\chi^{(3)}$ should experience a strong resonant enhancement. From the third-order perturbation calculation, we find

$$\chi^{(3)}(\omega=\omega_1-\omega_2-\omega_3) \cong \frac{N}{\hbar^3} \mu_{4s-5p} \; \mu_{5p-5s} \; \mu_{5s-4p} \; \mu_{4p-4s} A \qquad (34)$$

where $A = [(\omega_{5p-4s}-\omega_1-i\Gamma_1)(\omega_{5s-4s}-\omega_1+\omega_2+i\Gamma_2)(\omega_{4p-4s}-\omega_3)]^{-1}$. N is the density of K atoms, μ is the dipole moment operator, and Γ is the damping constant for a transition. The resonant frequencies and the matrix elements for the various transitions in potassium can be found in published tables.[49] If we take $N = 10^{17}/cm^3$, $\omega_{5p-4s}-\omega_1 = 50\ cm^{-1}$, we obtain from Eq. (34), $\chi^{(3)}(\omega) = 6 \times 10^{-10}$ esu. For each pump field at 100 esu (2.5 MW/cm^2), the corresponding nonlinear polarization is 6×10^{-4} esu, as compared, for example, with the second-order nonlinear polarization of $\sim 10^{-2}$ esu in $LiNbO_3$. The value of $\chi^{(3)}(\omega)$ does not vary appreciably with the infrared frequency ω. In principle, we can increase $\chi^{(2)}$ further by increasing N or decreasing $(\omega_{5p-4s}-\omega_1)$. There are clear advantages in using gas media for optical mixing: the threshold of optical breakdown is high, the length of the medium can be long, and the cost is less.

Knowing $\chi^{(3)}$, we can then calculate the infrared output using the results in Section II. In order to generate infrared radiation efficiently

in the optical mixing process, we must also have the phase matching condition satisfied. In this case, we would like to have collinear phase matching so that the coherent length is long and comparable to the length of the gas medium. The collinear phase matching condition can be written as[50]

$$\omega_1[n(\omega_1)-1] = \omega_2[n(\omega_2)-1] + \omega_3[n(\omega_3)-1] + \omega[n(\omega)-1] \qquad (35)$$

where n is the refractive index. Equation (35) can be satisfied over a certain frequency range with the help of anomalous dispersion. As seen from Fig. 11, ω_2 and ω are both far less than the frequency of any transition from the ground state to an excited state, and hence, $n(\omega_2)-1$ and $n(\omega)-1$ do not vary appreciably with ω_2 and ω. On the other hand, $n(\omega_3)-1$ with $\omega_{5p-4s} > \omega_3 > \omega_{4p-4s}$ is negative and may slowly vary with ω_3. Then, for fixed ω_3, we can vary ω_1 around the 4s→5p resonance and use the anomalous dispersion of $n(\omega_1)$ to satisfy the phase matching condition in Eq. (35). However, when ω becomes smaller and smaller, (resonant enhancement of $\chi^{(3)}$ requires $\omega+\omega_3 \approx \omega_{5s-4s}$), Eq. (35) is only satisfied with ω_1 farther away from the 4s→5p resonance, and $\chi^{(3)}$ decreases accordingly. This difficulty can be avoided by mixing Na as buffer gas into K vapor. Since ω_3 is close to the sodium D lines, the sodium vapor gives an appreciable contribution to $n(\omega_3)$. We can then have $\omega_1 \sim \omega_{5p-4s}$ fixed and vary the sodium concentration to achieve phase matching at a given ω_3.

The above scheme for generating tunable infrared radiation has been used by Sorokin et al.[50] They used a 100 kW N_2 laser to produce two collinear dye laser beams at ω_1 and ω_3 (1 kW at ω_1 and 10 kW at ω_3).

The two beams were focused into a heat pipe containing K vapor or a mixture of K and Na vapor. The ω_1 beam close to the 4s-5p resonance was intense enough to be able to generate an $\omega_2 = \omega_1 - \omega_{5s-4s}$ beam via stimulated Raman transitions 4s→5s in the vapor. By varying ω_3 and by varying ω_1 or the Na concentration to achieve collinear phase matching, they were able to detect infrared output tunable from 2 to 25 μm. The output power ranged from 100 mW at 2 μm to 0.1 mW at 25 μm. A tuning range extended to 100 μ and beyond is possible and a much higher output power is expected with stronger pump fields.[50]

An alternative method to generate tunable far-infrared radiation in metal vapor is to let ω_1 close to ω_{4p-4s} and $\omega_1+\omega_2 = \omega_{5s-4s}$. The third pump beam has a frequency $\omega_3 = \omega_1+\omega_2+\omega$. Then, the corresponding third-order nonlinear susceptibility is

$$\chi^{(3)}(\omega = -\omega_1-\omega_2+\omega_3) \cong \frac{N}{\hbar^3}\mu_{4s-4p}\,\mu_{4p-5s}\,\mu_{5s-5p}\,\mu_{5p-4s}\,A'$$

$$A' = [(\omega_{4p-4s}-\omega_1-i\Gamma_1)(\omega_{5s-4s}-\omega_1-\omega_2-i\Gamma_2)(\omega_{5p-4s}-\omega_3)]^{-1}. \qquad (36)$$

Again, $\chi^{(3)}(\omega)$ has strong resonant enhancement. The energy differences between levels in potassium are not ideal for the available dye lasers. Other metal vapors such as Sr, Mg, Cd, Zn, etc. are perhaps more appropriate for this scheme.[53] Experiments using this scheme have not yet been carried out, although the inverse process with $\chi^{(3)}(\omega_3=\omega_1+\omega_2+\omega)$ has already been reported.[53]

As a concluding remark, we should mention that there is possible difficulty in obtaining efficient far-infrared generation at long wavelengths in vapor. When the far-infrared wavelength becomes comparable with the beam diameter, diffraction loss over the long active length is

very strong. The efficiency should then appear to be greatly reduced from that calculated with simple plane wave approximation.

IX. FAR-INFRARED GENERATION BY PICOSECOND PULSES

We have so far assumed that the pump fields are monochromatic and that monochromatic far-infrared radiation is generated by **optical mixing**. With pulsed lasers as the pump sources, this is a good approximation as long as the pulse is long. The laser spectral width, limited by the pulsewidth, determines the spectral purity of the far-infrared output. If, however, the laser pulsewidth is as short as 1 psec, the corresponding laser spectral width should be at least 15 cm^{-1}. Then, even when there is only one such short pulse propagating in a nonlinear crystal, optical mixing of the various Fourier components of the pulse can generate far-infrared in the crystal.[54,55] This process can be considered as an optical rectification process, but here we are dealing only with the propagating component of the generated field and the far-infrared output is subject to influences of phase matching, diffraction, boundary reflections, radiation efficiency, etc.[54]

Far-infrared generation by short optical pulses is again governed by the wave equation

$$[\nabla x\ (\nabla x\vec{E}) + \frac{1}{c^2}\frac{\partial^2}{\partial t^2}\underset{\approx}{\varepsilon}\cdot\vec{E}\ ] = -\frac{4\pi}{c^2}\frac{\partial^2}{\partial t^2}\vec{P}^{NL}(r,t) \tag{37}$$

where $\vec{E}$ is the far-infrared field. The nonlinear polarization $\vec{P}^{NL}(\vec{r},t)$ is related to the pulsed laser field $E_\ell(\vec{r},t)$ by

$$\vec{P}^{NL}(\vec{r},t) = \underset{\approx}{\chi}^{(2)} : \vec{E}_\ell \vec{E}_\ell^{\,*}(\vec{r},t) \qquad (38)$$

if we neglect the dispersion of $\chi^{(2)}$. With dispersion, the expression of $\vec{P}^{NL}$ and hence the solution of Eq. (37) become more complicated. Anyway, given $\underset{\approx}{\chi}^{(2)}$ and $\vec{E}_\ell(\vec{r},t)$, we can in principle solve Eq. (37) with appropriate boundary conditions. We can then calculate the far-infrared output and its power spectrum. In practice, it is often easier to solve Eq. (37) through Fourier transform of $\vec{E}(\vec{r},t)$ and $\vec{P}^{NL}(\vec{r},t)$. This has been done for far-infrared generation in a thin slab of nonlinear crystal.[54] The solution is too complex to be reproduced here. We shall give only a physical description of the solution in the following.

In Fig. 12A, we show a calculated power spectrum of far-infrared radiation generated by a 2-psec Nd laser pulse from a 1 mm $LiNbO_3$ slab with the $\hat{c}$-axis perpendicular to the normal. The interference pattern under the dotted curve is due to the Fabry-Perot boundary condition of the slab. The dotted envelope curve has contributions mainly from three physical sources. They are plotted qualitatively in Fig. 12B. Curve a gives the power spectrum of the rectified input pulse. Curve b gives the variation of the dipole radiation efficiency with the far-infrared frequency ω; it has approximately an ω^2 dependence with a sharp cutoff as $\omega \to 0$ due to diffraction. Curve c is the phase-matching curve corresponding to phase matching at $\omega = 0$. It is essentially the product of these three curves which yields the dotted envelope of the power spectrum in Fig. 12A.

The theoretical calculations actually give a very good description of the experimental results.[56,57] Yang et al.[56] used mode-locked pulses from a Nd: glass laser to generate far-infrared radiation from a

0.775 mm $LiNbO_3$ crystal with the $\hat{c}$-axis perpendicular to the normal. The laser pulsewidth obtained by two-photon fluorescence measurement was about 5 psec. As shown in Fig. 13a, the observed far-infrared power spectrum is in good agreement with the theoretical one calculated by assuming a 1.8 psec pulsewidth. The Fabry-Perot pattern is absent here because the actual spectrum has been averaged over the instrumental resolution. The discrepancy in the pulsewidths is presumably due to the different nature of far-infrared generation and two-photon fluorescence measurements. If the laser pulse has some rapidly varying ripples on it, the two-photon fluorescence method would not see the ripples, but the far-infrared generation which measures the actual spectral content of the pulse would see an apparently shorter pulse.

We can orient the crystal to achieve phase matching at finite ω. We should then expect to find a peak in the output spectrum at the phase-matched frequency.[56] An example is shown in Fig. 13b. Again, the experimental results agree well with theory. The two peaks in the theoretical curve corresponds to phase matching with the far infrared propagating backward and forward respectively. Figure 13b suggests that we can have tunable far-infrared output by simply rotating the nonlinear crystal. With a laser peak power of 1 GW, the observed far-infrared output had a peak power of 250 W from a 1.5 mm $LiNbO_3$ crystal.

Since the generated far-infrared power spectrum is not the same as the power spectrum of the rectified laser pulse, the far-infrared pulse should have a different pulse shape than the laser pulse and is always longer. However, it is still in the picosecond range and can perhaps be used to investigate fast transient phenomena in the far-infrared region.

Auston et al.[48] have also been able to observe far infrared generation by optical rectification of picosecond pulses via impurity absorption in an acentric polar crystal. In their case, phase matching is not important because of the small active length limited by the strong absorption. The short pulse of the nonlinear polarization $P^{NL}(\vec{r},t)$ generated in the crystal can also be monitored in the form of a short electrical current pulse.[46] Electrical pulses as short as 10 psec have been observed.

X. GENERATION OF OTHER EXCITATIONAL WAVES BY OPTICAL MIXING

Aside from far-infrared radiation, other excitational waves can also be generated by optical mixing. Generation of acoustic waves by optical mixing, for example, is well known. With high-power laser beams as pump sources, acoustic waves generated by stimulated Brillouin scattering can readily be observed.[58] It is possible that one can construct a high-intensity tunable acoustic source by means of optical mixing. This is particularly interesting for the case of hypersonic waves at very high frequencies. Using a superlattice structure as the medium, we may be able to generate coherent hypersonic waves with frequencies much higher than 50 GHz.[59] The experimental feasibility of such a scheme has not yet been explored.

We can also use optical mixing to generate high-intensity spin waves, plasma waves, etc. The linear properties of these excitational waves are often fairly well understood, but their nonlinear properties, which are interesting in their own right, have never been studied extensively. The reason is that the intensities of these waves excited by the usual means are often not very high. It is therefore possible that generation of high-intensity excitational waves by optical mixing can lead to some

very interesting nonlinear problems. High excitations of plasma waves as a means to heat up a plasma for controlled fusion has recently been proposed.[60]

XI. OPTICAL MIXING AS A SPECTROSCOPIC TECHNIQUE

As we mentioned in the INTRODUCTION, one purpose of studying far-infrared generation by optical mixing is to find a better far-infrared source for far-infrared spectroscopy work. The far-infrared source is often used to excite and probe the low-frequency excitation in a medium. In many cases, however, we can use optical mixing directly as a spectroscopic technique to study the excitations in a medium.

Consider a slab of thickness ℓ in which the material excitation ψ with a resonant frequency ω_o is driven by $E(\omega_1)E^*(\omega_2)$.

$$\hbar(i\frac{\partial}{\partial t} - \omega_o + i\Gamma)\psi(\omega) = S^{(2)}E(\omega_1)E^*(\omega_2). \tag{39}$$

For simplicity, we assume a medium with inversion symmetry. A third field $E(\omega_3)$ is then used to interact with ψ and generate a new field $E(\omega_4)$ at $\omega_4 = \omega_3+\omega = \omega_3+\omega_1-\omega_2$. The wave equation for $E(\omega_4)$ is then given approximately by

$$\begin{aligned}[\nabla x(\nabla x) - \omega_4^2\varepsilon(\omega_4)/c^2]\vec{E}(\omega_4) &= (4\pi\omega_4^2/c^2)[\chi_\infty^{(3)}\vec{E}(\omega_3)\vec{E}(\omega_1)\vec{E}^*(\omega_2) \\ &\quad -S^{(2)*}(\rho_g-\rho_f)\vec{E}(\omega_3)\psi(\omega)] \\ &= (4\pi\omega_4^2/c^2)\chi^{(3)}E(\omega_3)E(\omega_1)E(\omega_2) \end{aligned} \tag{40}$$

$$\chi^{(3)}(\omega_4=\omega_3+\omega_1-\omega_2) = \chi_\infty^{(3)} - |S^{(2)}|^2(\rho_g-\rho_f)/\hbar(\omega-\omega_o+i\Gamma)$$

where ρ_g and ρ_f are the populations in $\langle g|$ and $\langle f|$ respectively. With the approximation of slowly varying amplitude, the solution of Eq. (40) at phase matching $\vec{k}_4 = \vec{k}_3+\vec{k}_1-\vec{k}_2$ yields

$$|E(\omega_4)|^2 = (2\pi\omega_4^2/c^2k_{4z})^2|\chi^{(3)}|^2\ell^2|E(\omega_1)|^2|E(\omega_2)|^2|E(\omega_3)|^2. \qquad (41)$$

Thus the signal $|E(\omega_4)|^2$ as a function of $\omega = \omega_1-\omega_2$ from this optical mixing process gives direct information about the dispersion of $\chi^{(3)}(\omega_4)$, especially the resonant structure of $\chi^{(3)}(\omega_4)$. If the dispersion of $\chi_\infty^{(3)}$ around $\omega \sim \omega_o$ is negligible, the maximum and minimum of $|\chi^{(3)}|$ occur at $\omega_\pm = (\omega_1-\omega_2)_\pm$ respectively with

$$\omega_\pm = \omega_o + \frac{a}{2\chi_\infty^{(3)}} \pm \left[\left(\frac{a}{2\chi_\infty^{(3)}}\right)^2 + \Gamma^2\right]^{1/2} \qquad (42)$$

where $a = |S^{(2)}|^2(\rho_g-\rho_f)/\hbar$. An example of $|\chi^{(3)}(\omega_4)|^2$ vs ω around ω_o is shown in Fig. 14. From the measured values of $\omega_\pm$, $\chi_{max}^{(3)}$, and $\chi_{min}^{(3)}$, we can in principle obtain values for ω_o, Γ, a, and $\chi_\infty^{(3)}$. Therefore, such a nonlinear spectroscopic technique is clearly useful to probe not only the linear characteristics of the resonant excitation in the medium, but also the nonresonant nonlinear optical properties (described by $\chi_\infty^{(3)}$) of the medium.

Wynne[61] and Bloembergen and coworkers[62,63] have demonstrated experimentally the potential of this spectroscopic technique. Using two N_2-laser-pumped dye lasers as the tunable sources ($\omega_1 = \omega_3 \neq \omega_2$),

Levenson and Bloembergen[63] have probed the resonant structure around the Raman-active modes and measured $\chi_{\infty}^{(3)}$ in a number of liquids and solids. The same technique can of course be used to probe the resonant structure around other types of elementary excitations in a medium.[64]

We can also use optical mixing to study the dynamic properties of a material excitation. Suppose the driving force $E(\omega_1)E^*(\omega_2)$ for $\psi(\omega)$ in Eq. (39) is in the form of a short pulse, shorter than or comparable with $1/\Gamma$. Then, the time-dependent solution of Eq. (39) describes the transient response of $\psi(\omega)$ to the driving pulse. If we wait long enough after the driving pulse is over, ψ will eventually decay exponentially as $\exp(-t/T_2)$. Here, $T_2 \equiv 1/\Gamma$ is a characteristic relaxation time of the coherent excitational wave $\psi(\omega)$, and is often known as the transverse relaxation time. We can probe the time variation of $\psi(\omega)$ by using a third beam $E(\omega_3)$ to beat coherently with ψ and generate a signal $E(\omega_4)$ at $\omega_4 = \omega+\omega_3$. From the time dependence of $|E(\omega_4)|^2$, we can then measure T_2 directly. It is also possible if the pulsed fields $E(\omega_1)$ and $E(\omega_2)$ are sufficiently intense, to induce through two-photon transitions an appreciable change in the population difference $(\rho_g-\rho_f)$. Again, after the driving pulse is over, $(\rho_g-\rho_f)$ will finally decay exponentially. In this case, however, the characteristic relaxation time is T_1, often known as the longitudinal relaxation time. We can again use a third beam $E(\omega_3)$ to probe the time variation of $(\rho_g-\rho_f)$ by simply monitoring the spontaneous anti-Stokes Raman scattering signal at $\omega_4 = \omega_3+\omega$ as a function of time.

DeMartini and Ducuing[65] first used the method to measure T_1 of the vibration excitation of gaseous H_2. In liquids and solids, T_1 and T_2

of vibrational excitations are usually in the picosecond range. Using picosecond mode-locked pulses, Alfano and Shapiro[66] and Kaiser and his coworkers[67] have recently been able to measure T_1 and T_2 for vibrational excitations in a number of liquids and solids. In their cases, $E(\omega_2)$ is automatically generated by the pump pulse $E(\omega_1)$ in the medium via stimulated Raman scattering. The analysis is somewhat more complicated but the physics involved is the same. They have also been able to use the technique to find the decay routes of a vibrational excitation.[68] Extension of the method to other types of excitations is clearly possible. In fact, this has so far been the only method one can use to measure directly relaxation times of excitations in the picosecond range.

XII. CONCLUSION

We have described in the previous sections the many different ways of generating far-infrared radiation by optical mixing. We now summarize in Table I the present experimental status of the various potentially hopeful methods. The values quoted in the Table are what have been reported so far. In many cases, they can easily be improved by using higher input laser powers.

A glance at the Table shows that compared with blackbody source, the far-infrared radiation generated by optical mixing has not only a much higher peak power, but also a larger average power. Besides, its spectral purity is only limited by the input laser linewidths. Experiments on far-infrared generation are still in the beginning stage. More sophisticated schemes are yet to be tried out. In the near future, we can anticipate that optical mixing will yield far-infrared radiation with even much higher power, better spectral purity, and wider tunability.

Then, the field of far-infrared spectroscopy will certainly be quite different from what it is now.

ACKNOWLEDGEMENT

This paper was written with the partial support of the U.S. Atomic Energy Commission and the Center for Theoretical Studies of the University of Miami.

REFERENCES

1. See, for example, G. Rosen and F. C. Whitmore, Phys. Rev. 137B, 1357 (1965).
2. See, for example, N. Bloembergen, Nonlinear Optics (W. A. Benjamin, Inc., New York, 1965).
3. See, for example, Spectroscopic Techniques for Far Infrared, Submillimeter, and Millimeter Waves, D. H. Martin, Ed. (North-Holland Publishing Co., Amsterdam, 1967).
4. P. L. Richards, Far-Infrared Properties of Solids, S. Mitra, Ed. (Plenum Press, 1970) p. 103;
   Y. Taur, Ph.D. Thesis, (University of California, Berkeley, 1974).
5. D. W. Faries, K. A. Gehring, P. L. Richards, and Y. R. Shen, Phys. Rev. 180, 363 (1969); D. W. Faries, P. L. Richards, Y. R. Shen, and K. H. Yang, Phys. Rev. A3, 2148 (1971).
6. K.H. Yang, J. R. Morris, P. L. Richards, and Y. R. Shen, Appl. Phys. Letters 23, 669 (1973).
7. B. Lax, R. L. Aggarwal, and G. Favrot, Appl. Phys. Letters 23, 679 (1973).
8. B. Lax and R. L. Aggarwal, J. Opt. Soc. Am. 64, 533 (1974).
9. Reported by A. L. Robinson in Science 184, 1064 (1974).
10. J. A. Armstrong, N. Bloembergen, J. Ducuing, and P. S. Pershan, Phys. Rev. 127, 198 (1962).
11. See, for example, J. D. Jackson, Classical Electrodynamics (J. Wiley & Sons, Inc., New York, 1962) Chapter 9.

12. D. W. Faries, Ph.D. Thesis, University of California, Berkeley (1969).

13. J. E. Bjorkholm, Phys. Rev. 142, 126 (1966).

14. D. A. Kleinman, A. Ashkin, and G. D. Boyd, Phys. Rev. 145, 338 (1966).

15. J. Morris and Y. R. Shen, (to be published).

16. F. Zernike and P. R. Bermann, Phys. Rev. Letters 15, 999 (1965).

17. F. Zernike, Bull. Am. Phys. Soc. 12, 687 (1967); Phys. Rev. Letters 22, 931 (1969).

18. T. Y. Chang, V. T. Nguyen, and C. K. N. Patel, Appl. Phys. Letters 13, 357 (1968); T. J. Bridges and T. Y. Chang, Phys. Rev. Letters 22, 811 (1969).

19. C. K. N. Patel and V. T. Nguyen, Appl. Phys. Letters 15, 189 (1969); V. T. Nguyen and C. K. N. Patel, Phys. Rev. Letters 22, 463 (1969).

20. V. T. Nguyen, A. R. Strnad, A. M. Jean-Louis, and G. Duroffoug, in The Physics of Semimetals and Narrow Gap Semiconductors, D. L. Carter and R. T. Bates, Eds. (Pergamon Press, New York, 1971) p. 231.

21. T. J. Bridges and A. R. Strnad, Appl. Phys. Letters 20, 382 (1972).

22. G. D. Boyd, T. J. Bridges, C. K. N. Patel, and E. Buchler, Appl. Phys. Letters 21, 553 (1972).

23. V. T. Nguyen and T. J. Bridges, Phys. Rev. Letters 29, 359 (1972).

24. T. Yajima and K. Inoue, IEEE J. Quantum Electronics QE-4, 319 (1968); QE-5, 140 (1969); Phys. Letters 26A, 281 (1968).

25. J. M. Yarborough, S. S. Sussman, H. E. Puthoff, R. H. Pantell, and B. C. Johnson, Appl. Phys. Letters 15, 102 (1969).

26. S. Biraud and G. Chartier, Phys. Letters 30A, 177 (1969).

27. V. T. Nguyen and T. J. Bridges, Phys. Rev. Letters 29, 359 (1972); T. J. Bridges and V. T. Nguyen, Appl. Phys. Letters 23, 107 (1973);

V. T. Nguyen and T. J. Bridges, Proceedings of the Laser Spectroscopy Conference, Vail, Colorado, June 1973 (to be published).

28. P. P. Sorokin, J. J. Wynne, and J. R. Lankard, Appl. Phys. Lett. 22, 342 (1973); J. J. Wynne, P. P. Sorokin, and J. R. Lankard, in Proceedings of the Laser Spectroscopy Conference, Vail., Colo., June 1973 (to be published).

29. The optical properties of $LiNbO_3$ have been extensively studied in A. S. Barker and R. Louden, Phys. Rev. 158, 433 (1967); G. D. Boyd, R. C. Miller, K. Nassau, W. L. Bond, and A. Savage, Appl. Phys. Letters 5, 234 (1964); J. D. Axe and D. F. O'Kane Appl. Phys. Letters 9, 58 (1966).

30. F. DeMartini, Phys. Letters 30A, 319 (1969); 30A, 547 (1969); Phys. Rev. B4, 4556 (1971).

31. N. Bloembergen and Y. R. Shen, Phys. Rev. 133, A37 (1964); Y. R. Shen and N. Bloembergen, Phys. Rev. 137, A1787 (1965).

32. M. Born and K. Huang Dynamical Theory of Crystal Lattices (Clarendon Press, Oxford, 1954), Chapter II; K. Huang, Proc. Roy. Soc. (London) A208, 352 (1951); J. J. Hopfield, Phys. Rev. 112, 1555 (1958).

33. I. P. Kaminow and W. D. Johnson, Phys. Rev. 160, 519 (1967).

34. W. L. Faust and C. H. Henry, Phys. Rev. Letters 17, 1265 (1966); W. L. Faust, C. H. Henry, and R. H. Eick, Phys. Rev. 173, 781 (1968).

35. S. S. Sussman, Microwave Lab. Report No. 1851, Stanford Univ., 1970.

36. R. Loudon, Proc. Phys. Soc. (London) 82, 393 (1963).

37. P. N. Butcher, R. Loudon, and T. P. McLean, Proc. Phys. Soc. (London) 85, 565 (1965).

38. Y. R. Shen, Phys. Rev. 138, A1741 (1965).

39. C. H. Henry and C. G. B. Garrett, Phys. Rev. 171, 1058 (1968).

40. F. De Martini, J. Appl. Phys. 37, 12 (1966); Nuovo Cimento 51B, 16 (1967).

41. S. K. Kurtz and J. A. Giordmaine, Phys. Rev. Letters 22, 192 (1969); J. Gelbwachs, R. H. Pantell, H. E. Puthoff, and J. M. Yarborough, Appl. Phys. Letters 14, 258 (1969).

42. Y. R. Shen, Appl. Phys. Letters 23, 516 (1973).

43. T. L. Brown and P. A. Wolff, Phys. Rev. Letters 29, 362 (1972).

44. See, for example, C. K. N. Patel, in Fundamental and Applied Laser Physics, M. S. Feld, A. Javan, and N. A. Kurmit, Eds. (J. Wiley & Sons, Inc., 1973) p. 689 and the references therein; B. Lax, in Proceedings of the XI International Conference on the Physics of Semiconductors, Warsaw (Elsevier Book Co., Amsterdam, 1972) p. 1115, and the references therein.

45. D. H. Auston, A. M. Glass, and A. A. Ballman, Phys. Rev. Letters 28, 897 (1972).

46. D. H. Auston and A. M. Glass, Appl. Phys. Letters 20, 398 (1972).

47. A. M. Glass and D. H. Auston, Optics Comm. 5, 45 (1972).

48. D. H. Auston, A. M. Glass, and P. LeFur, Appl. Phys. Letters 23, 47 (1973).

49. R. B. Miles and S. E. Harris, IEEE J. Quantum Electronics QE-9, 470 (1973) and the references therein.

50. P. P. Sorokin, J. J. Wynne, and J. R. Lankard, Appl. Phys. Letters 22, 342 (1973); J. J. Wynne, P. P. Sorokin, and J. R. Lankard, Proceedings of the Laser Spectroscopy Conference, Vail, Colorado, June 25, 1973 (to be published).

51. J. F. Young, G. C. Bjorklund, A. H. Kung, R. B. Miles, and S. E. Harris, Phys. Rev. Letters 27, 1551 (1971); A. H. Kung, J. F. Young, G. C. Bjorklund, and S. E. Harris, Phys. Rev. Letters 29, 985 (1972);

A. H. Kung, J. F. Young, and S. E. Harris, Appl. Phys. Letters 22, 301 (1973).

52. R. T. Hodgson, P. P. Sorokin, and J. J. Wynne, Phys. Rev. Letters 32, 343 (1974).

53. S. E. Harris and D. M. Bloom, Appl. Phys. Letters 24, 229 (1974); D. M. Bloom, J. T. Yardley, J. F. Young, and S. E. Harris, Appl. Phys. Letters 24, 427 (1974).

54. J. R. Morris and Y. R. Shen, Optics Comm. 3, 81 (1971).

55. T. K. Gustafson, J.-P.E. Taran, P. L. Kelley, and R. Y. Chiao, Optics Comm. 2, 17 (1970).

56. K. H. Yang, P. L. Richards, and Y. R. Shen, Appl. Phys. Letters 19, 285 (1971).

57. T. Yajima and N. Takeuchi, Jap. J. Appl. Phys. 10, 907 (1971).

58. R.Y. Chiao, C. H. Townes, and B. P. Stoicheff, Phys. Rev. Letters 12, 592 (1964).

59. K. H. Yang, P. L. Richards, and Y. R. Shen, J. Appl. Phys. 44, 1417 (1973).

60. B. I. Cohen, A. N. Kaufman, and K. M. Watson, Phys. Rev. Letters 29, 581 (1973).

61. J. J. Wynne, Phys. Rev. Letters 29, 650 (1972); Phys. Rev. B6, 534 (1972).

62. M. D. Levenson, C. Flytzanis, and N. Bloembergen, Phys. Rev. B6, 3462 (1972); E. Yablonovitch, C. Flytzanis, and N. Bloembergen, Phys. Rev. Letters 29, 865 (1972).

63. M. D. Levenson, IEEE J. Quantum Electronics (to be published); M. D. Levenson and N. Bloembergen, (to be published).

64. S. E. Kramer, F. G. Parsons, and N. Bloembergen, Phys. Rev. B9, 1853 (1974).

65. F. DeMartini and J. Ducuing, Phys. Rev. Letters 17, 117 (1966).

66. R. R. Alfano and S. L. Shapiro, Phys. Rev. Letters 26, 1247 (1971).

67. D. von der Linde, A. Laubereau, and W. Kaiser, Phys. Rev. Letters 26, 954 (1971); A. Laubereau, D. von der Linde and W. Kaiser, Phys. Rev. Letters 27, 802 (1971); A. Laubereau, D. von der Linde, and W. Kaiser, Phys. Rev. Letters 28, 1162 (1972); A. Laubereau, D. von der Linde, and W. Kaiser, Opt. Comm. 7, 173 (1973).

68. R. R. Alfano and S. L. Shapiro, Phys. Rev. Letters 29, 1655 (1972); A. Laubereau, D. von der Linde, and W. Kaiser (to be published).

FIGURE CAPTIONS

Fig. 1. Schematic of a typical experimental arrangement for measurements of far-infrared generation. S1 and S2 are infrared spectrometers and PD1 and PD2 are infrared detectors.

Fig. 2. Dispersion of the polariton modes (heavy lines) as a result of coupling between electromagnetic waves) and the material excitational waves. In the absence of coupling, the polariton modes reduce to pure em modes (fine line labeled by $\omega = c\kappa/\sqrt{\varepsilon(\infty)}$) and the pure material excitations (fine horizontal line at ω_T), (after C. Kittel, Introduction to Solid State Physics, 4th Ed. J. Wiley, 1971) p. 186.

Fig. 3. Magnitude of the nonlinear susceptibility $\chi^{(2)}(\omega = \omega_1-\omega_2)$ versus ω around the 366 cm^{-1} lattice mode of GaP. $|\chi^{(2)}(\omega)|$ is normalized to 1 for large ω. The frequency ω_1 corresponds to 6328 Å of a He-Ne laser (after W. Faust and C. H. Henry, Phys. Rev. Letters 17, 1263 (1966), Fig. 2).

Fig. 4. Magnitude of $\chi^{(2)}_{zzz}(\omega = \omega_1-\omega_2)$ versus ω around the 248 cm^{-1} lattice mode of $LiNbO_3$. The frequency ω_1 corresponds to 6943 Å of a ruby laser.

Fig. 5. Theoretical curves and experimental data points of the relative IR output arising from phase-matched processes and the corresponding nonlinear susceptibility $|d|(\equiv|\chi^{(2)}|)$ as functions of the infrared wavelength (after F. DeMartini, Phys. Rev. B4, 4556 (1971), Fig. 9).

Fig. 6. Far-infrared power generated versus frequency for two phase-matching conditions. The far-infrared power is normalized by a sum-frequency power. The solid curves are the theoretical calculations based on data of the far-infrared absorption and the Raman cross section in $LiNbO_3$. The inset shows the experimental geometry for noncollinear phase matching (after Ref. 6, Fig. 2).

Fig. 7. Fig. 7 (a) Relative parametric gain G_{max} versus the IR frequency ω for GaP around the 366 cm^{-1} lattice mode. The solid portion of the curve indicates the frequency range over which phase matching is possible. (b) Infrared absorption coefficient for GaP. (c) Ratio of the infrared intensity $S_1(\omega)$ to the Stokes intensity $S_2(\omega_2)$ ($|\mathcal{E}(\omega)/\mathcal{E}(\omega_2)|^2$) (after C. H. Henry and C. G. B. Garrett, Phys. Rev. 171, 1058 (1968), Fig. 2).

Fig. 8. Parametric gain G_{max} and ratio of the infrared intensity to the Stokes intensity $P(\omega)/P_2(\omega_2)$ as functions of the infrared frequency around the 248 cm^{-1} lattice mode of $LiNbO_3$ (after Ref. 35, Fig. 4.5 and Fig. 4.6).

Fig. 9. Theoretical results (crosses) of normalized far-infrared power output in optical mixing as a function of $(\omega - \omega_o)/\Gamma$ in comparison with the experimental results of V. T. Nguyen and T. J. Bridges, Phys. Rev. Letters 29, 359 (1972) (after Ref. 42, Fig. 1).

Fig. 10. Theoretical curves of the Raman gain g, and the ratios of the far-infrared output $P(\omega)$ to the Raman output $P(\omega_2)$ for the collinear phase-mismatched case and for the noncollinear phase-matched case. The parameters used in the calculations are given in the text (after Ref. 42, Fig. 2).

Fig. 11. Energy level diagram of potassium and the infrared generation process.

Fig. 12 (A) The calculated far-infrared output spectrum for a 2 psec. Nd laser pulse normally incident on a 1 mm $LiNbO_3$ slab. The crystal is oriented with the c-axis parallel to the plane surfaces of the slab, and the laser pulse is polarized along the c-axis (after Ref. 54, Fig. 1).

(B) Curves showing the three major contributions to the far-infrared output spectrum in Fig. 12(A). Curve (a) gives the power spectrum of the rectified input pulse. Curve (b) gives the dipole radiation efficiency. Curve (c) gives the phase-matching effect for phase matching at $\omega = 0$.

Fig. 13 (a) Far-infrared spectrum generated by mode-locked pulses in $LiNbO_3$ phase matched at zero frequency. The experimental points were obtained from the Michelson interferogram and the solid curve from a theoretical calculation assuming Gaussian laser pulses with a 1.8-psec pulsewidth. (b) Far-infrared spectrum generated by mode-locked pulses in $LiNbO_3$ oriented to have forward and backward phase matching at 13.5 and 6.7 cm^{-1}, respectively. The experimental points were obtained from the Michelson interferogram. The solid and dashed curves were calculated by assuming Gaussian laser pulses with a pulse-width of 2.3 and 1.8 psec, respectively (after Ref. 56, Fig. 1).

Fig. 14. Typical results for the antiStokes intensity at ω_4 in calcite using the wave-mixing nonlinear spectroscopic technique. The polarizations were perpendicular to the optical axis of calcite (after M. D. Levenson, IEEE J. Quantum Electronics, to be published).

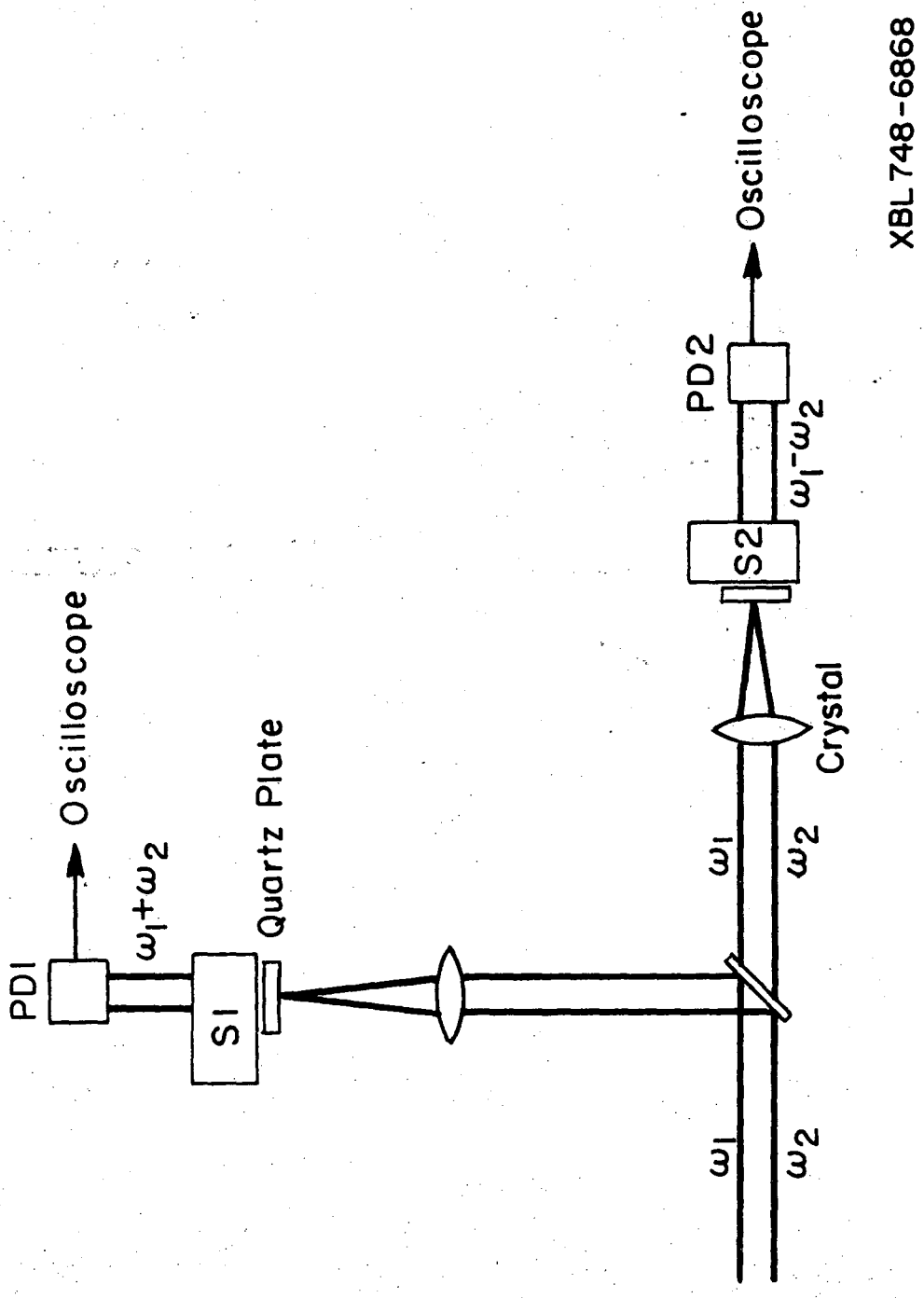
Oscilloscope
PD1
$\omega_1+\omega_2$
S1
Quartz Plate
ω_1
ω_2
Crystal
S2
$\omega_1-\omega_2$
PD2
Oscilloscope
XBL 748-6868

Fig. 1

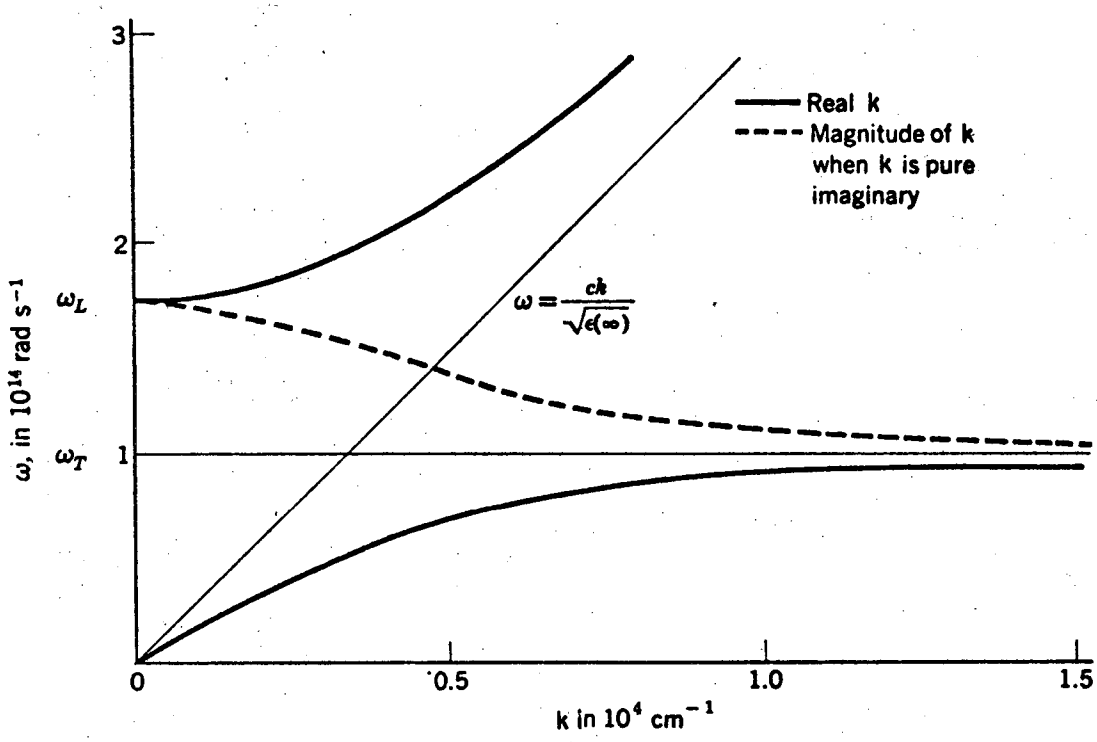

XBL748-6874

Fig. 2

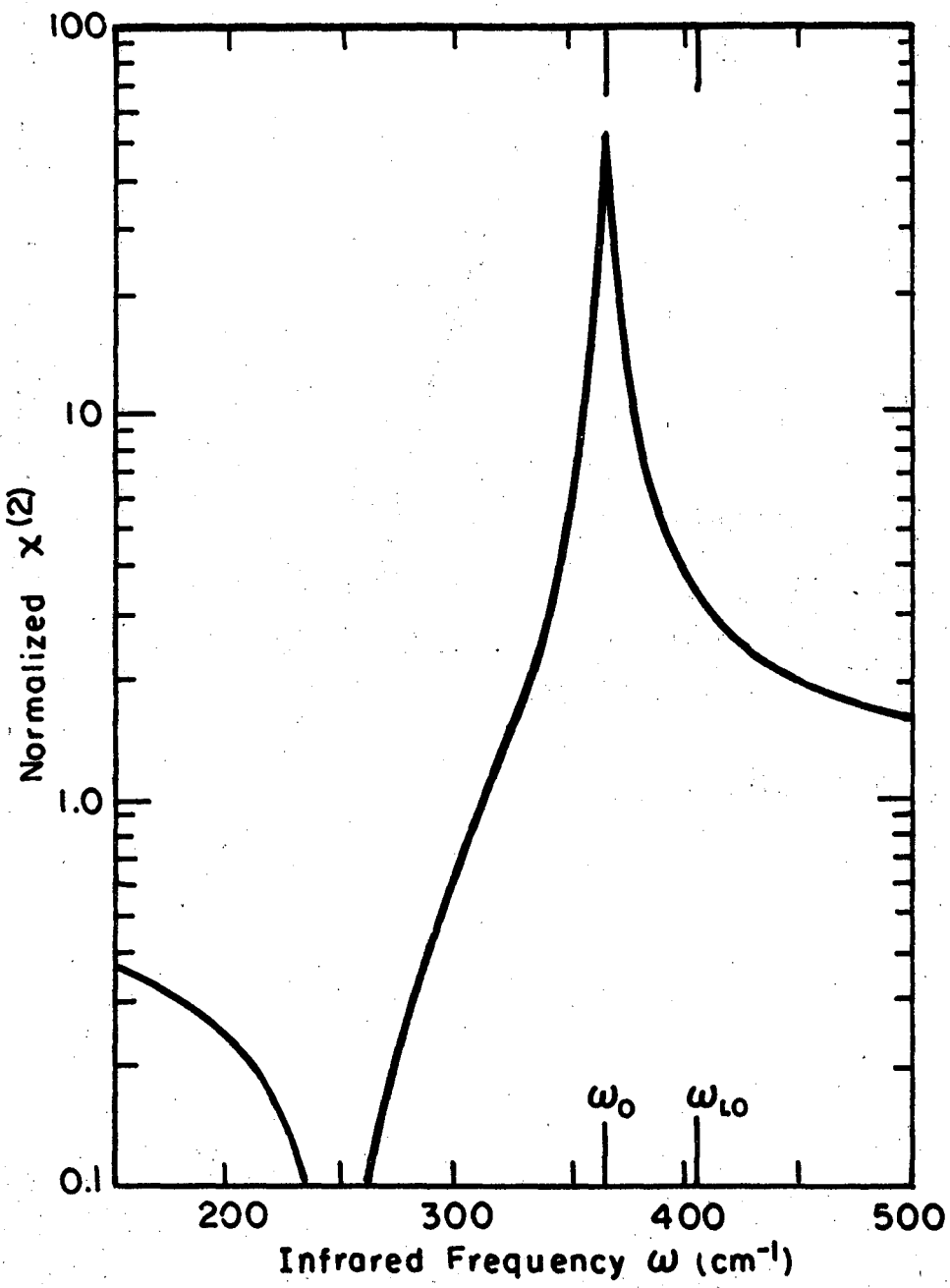

XBL 748-6872

Fig. 3

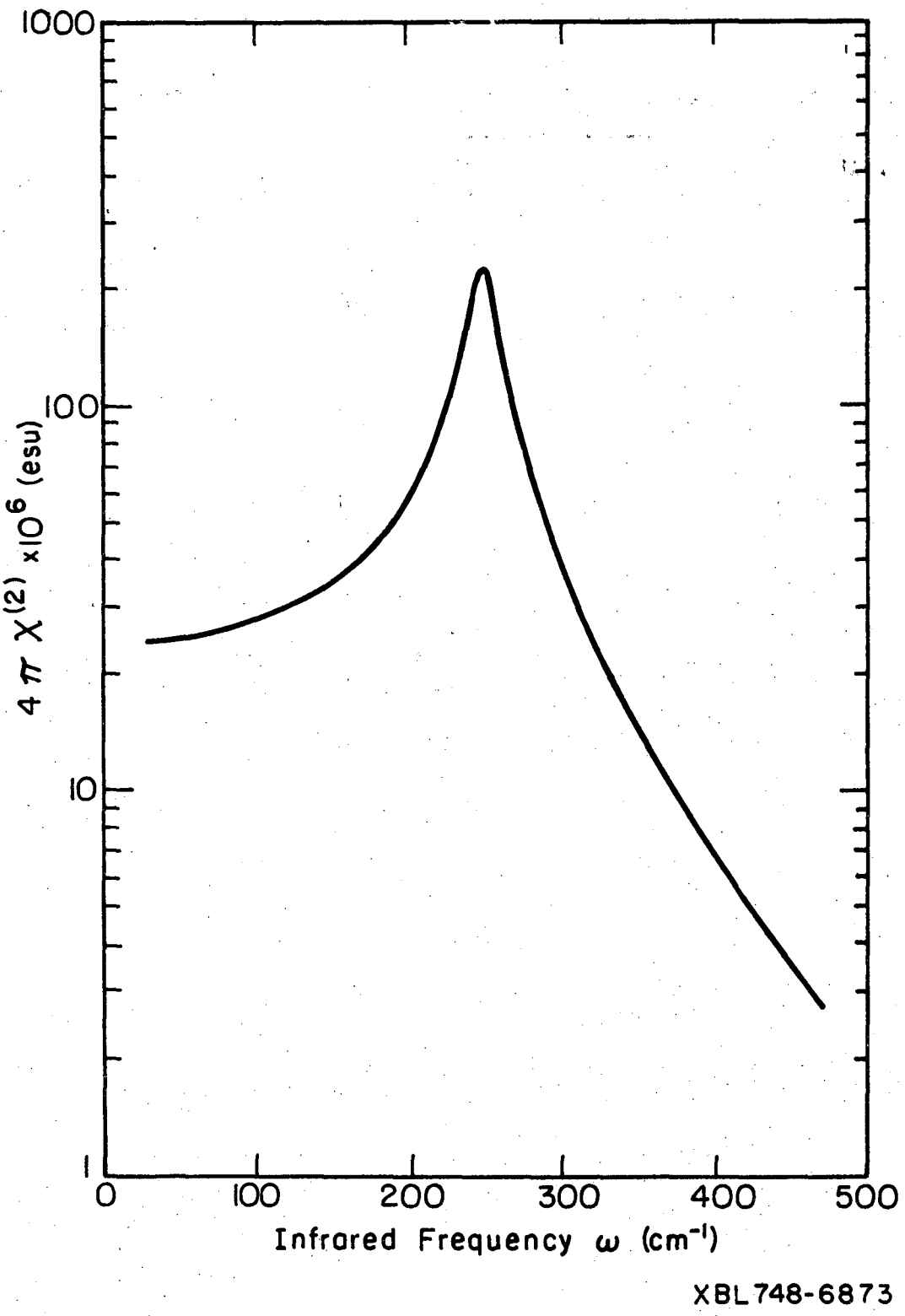
1000
100
10
1
0
100
200
300
400
500
$4\pi\chi^{(2)} \times 10^6$ (esu)
Infrared Frequency ω (cm^{-1})
XBL748-6873

Fig. 4

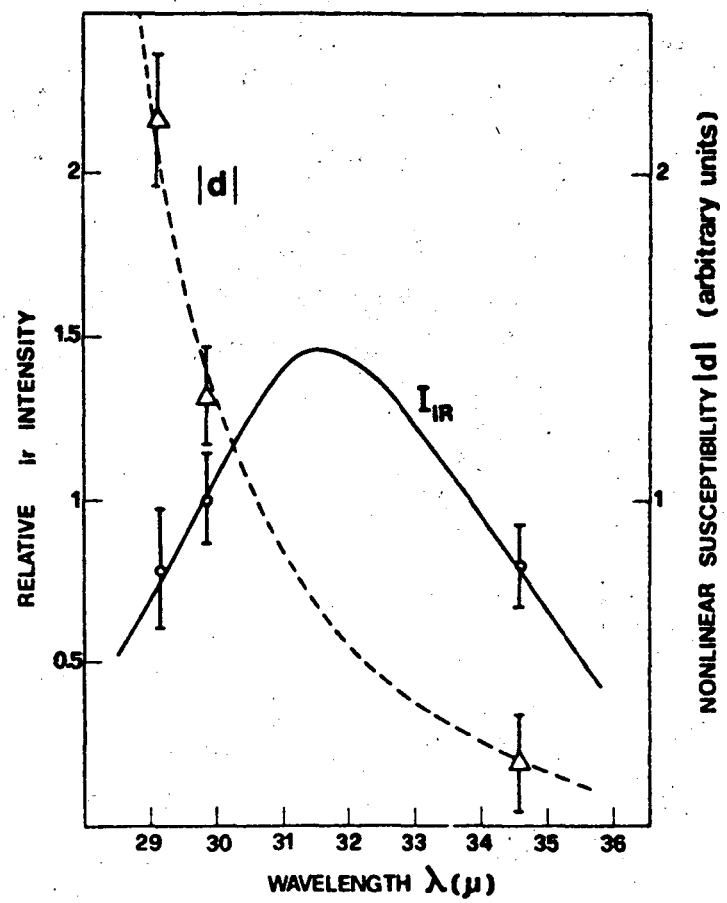

XBL 748-6953

Fig. 5

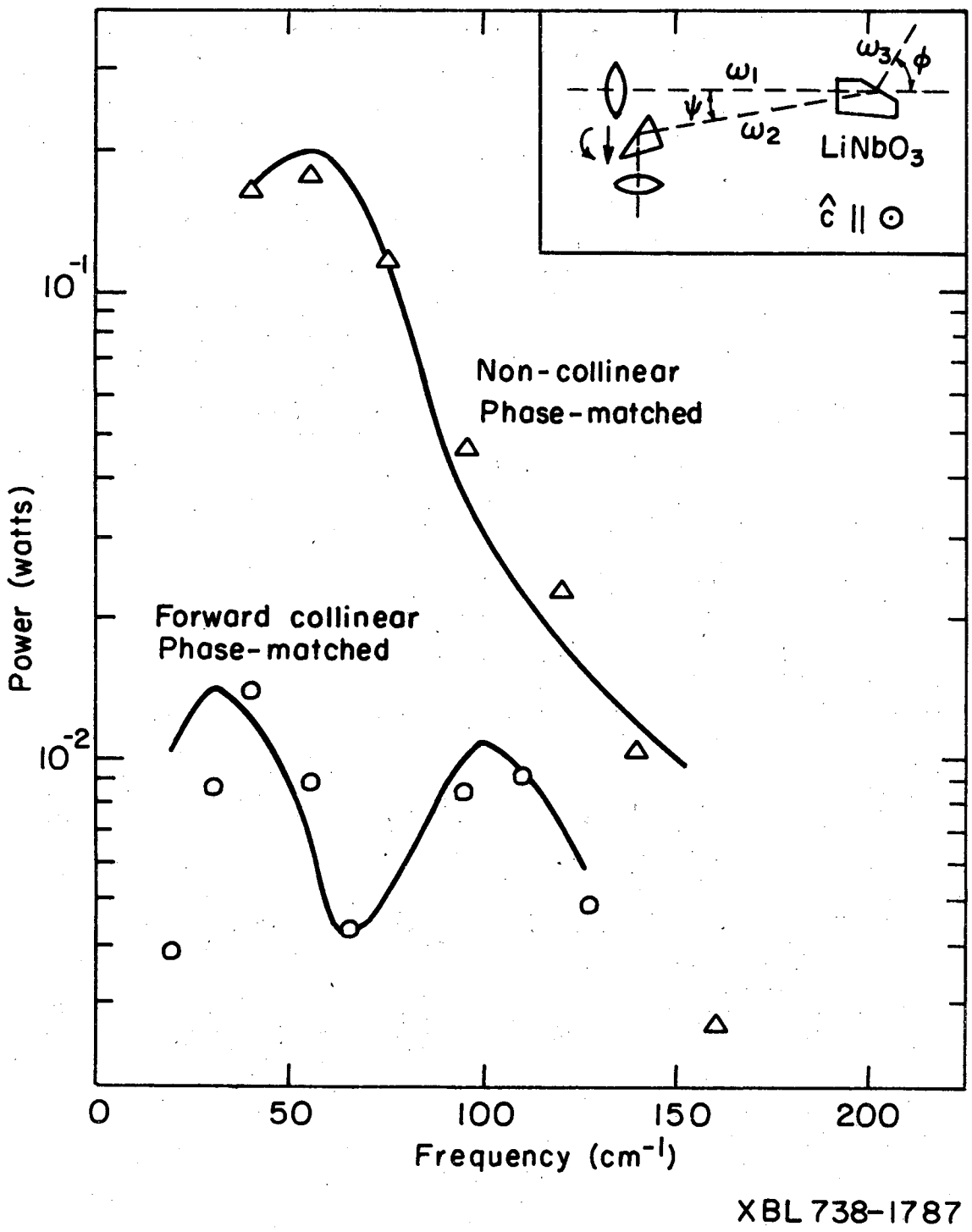

XBL 738-1787

Fig. 6

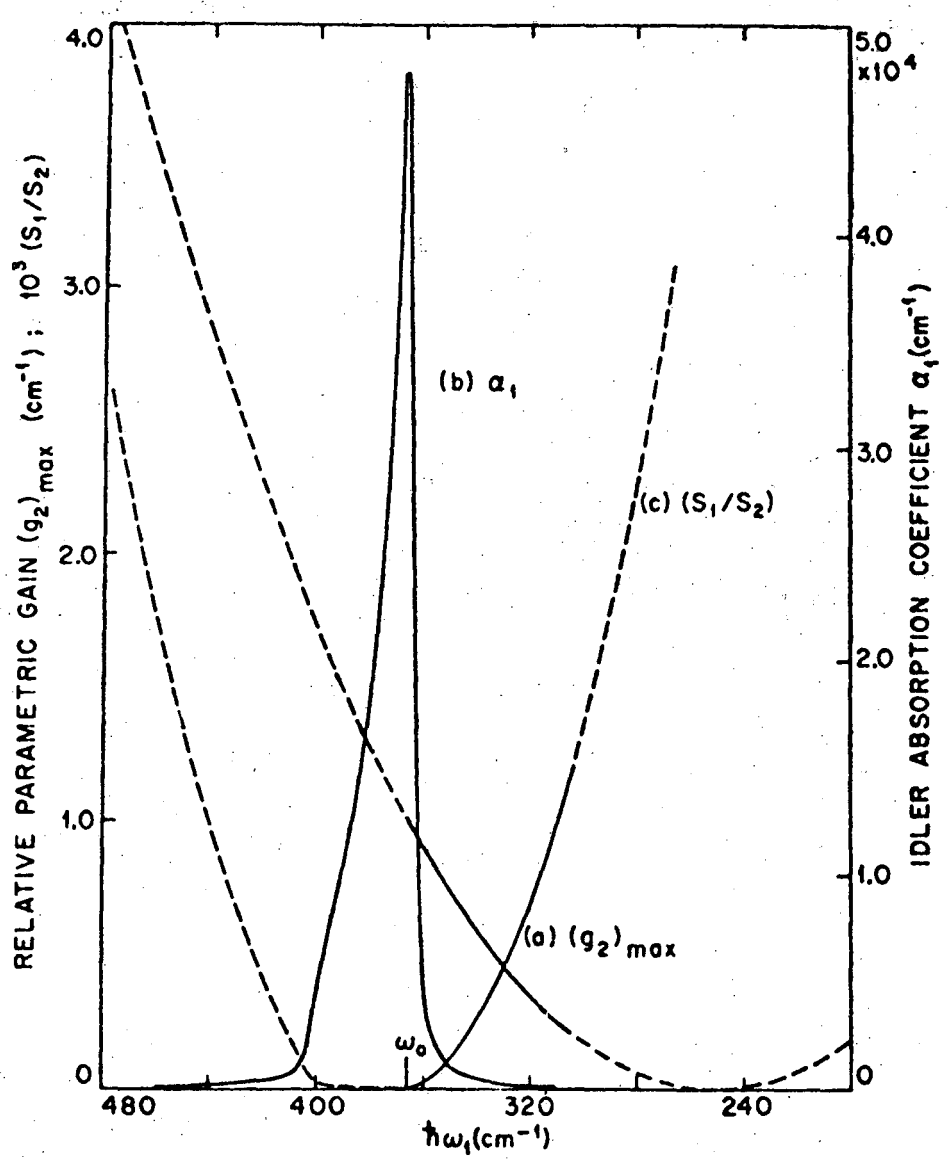

XBL 743-5799

Fig. 7

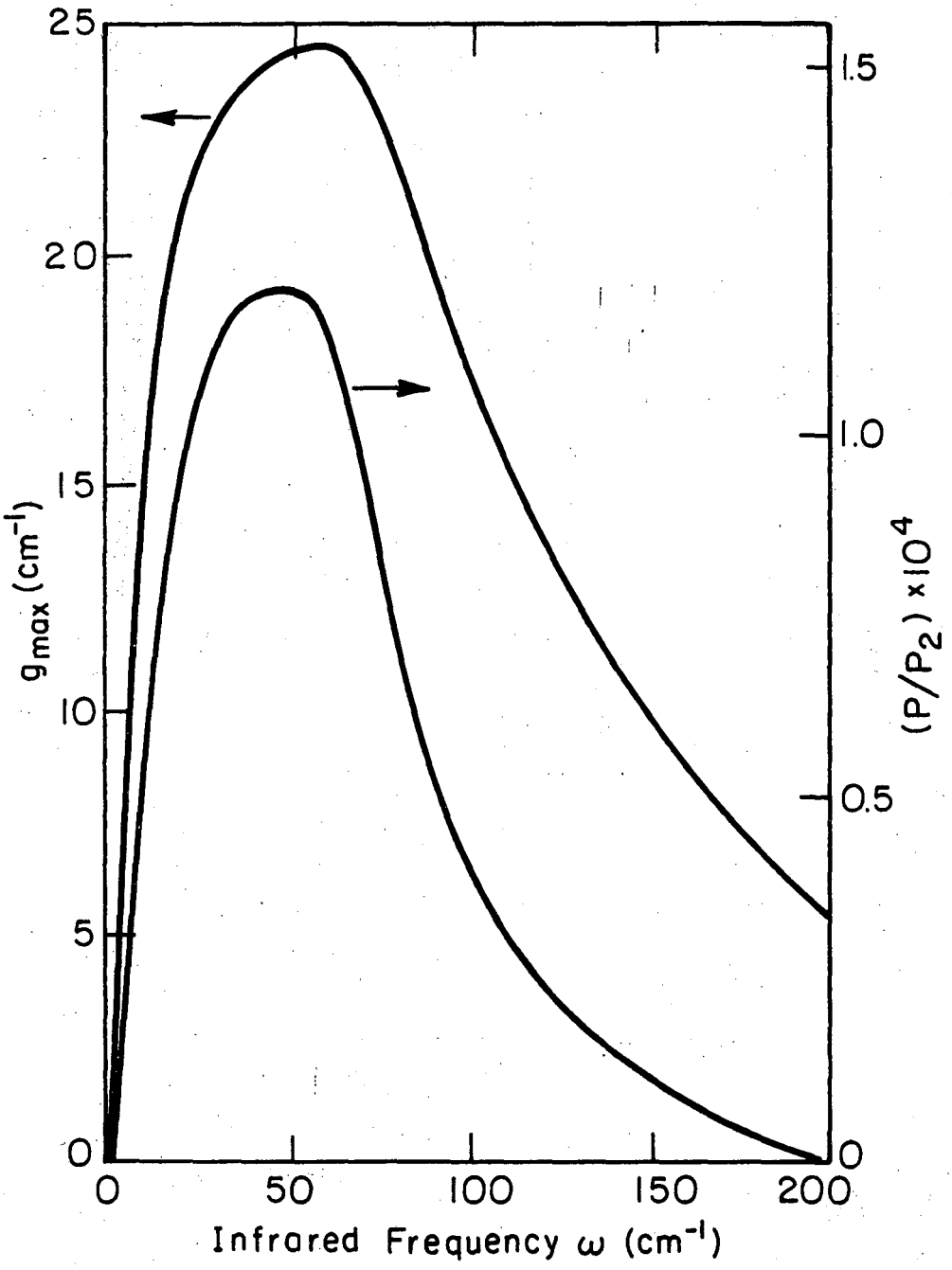

XBL 748-6870

Fig. 8

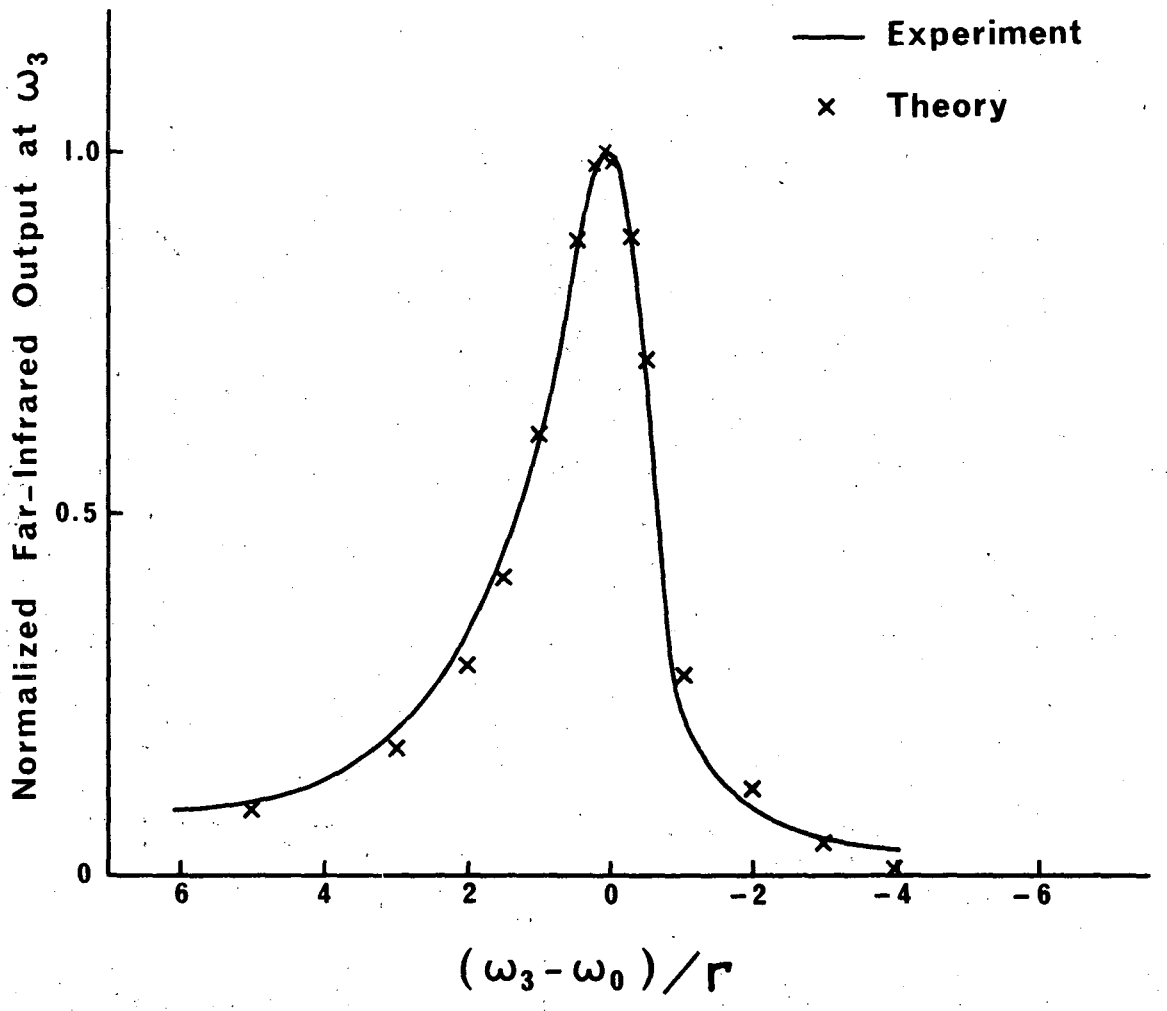

XBL 748-6952

Fig. 9

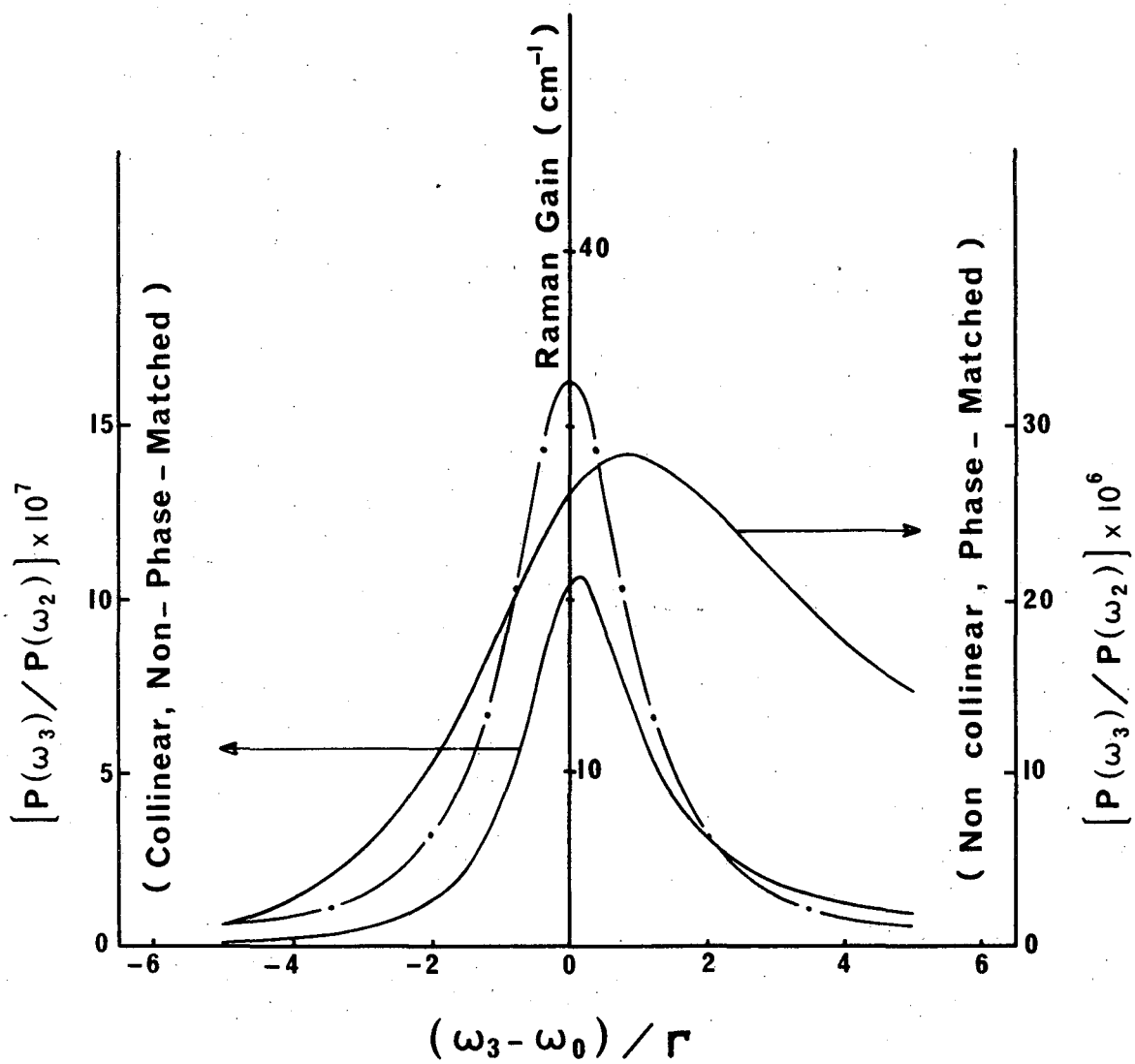

XBL 743-5795

Fig. 10

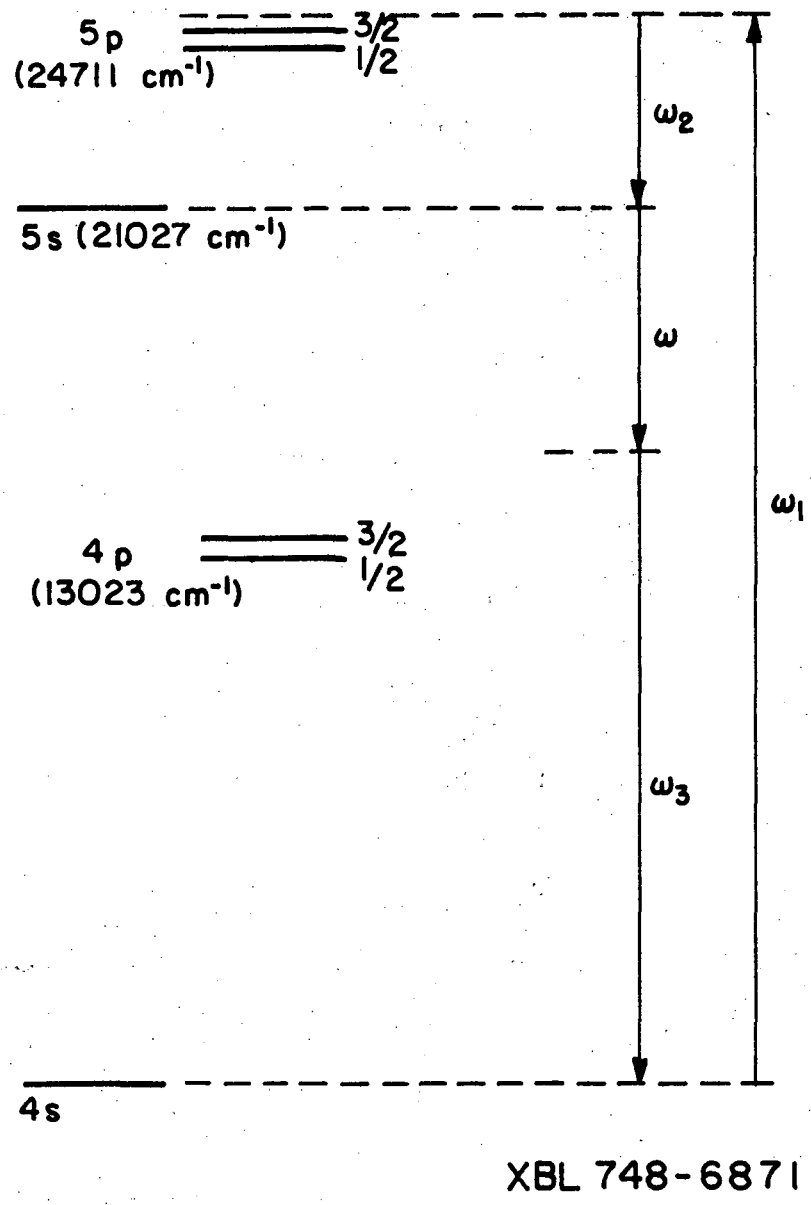
5p
(24711 cm⁻¹)
3/2
1/2
ω2
5s (21027 cm⁻¹)
ω
ω1
4p
(13023 cm⁻¹)
3/2
1/2
ω3
4s
XBL 748-6871

Fig. 11

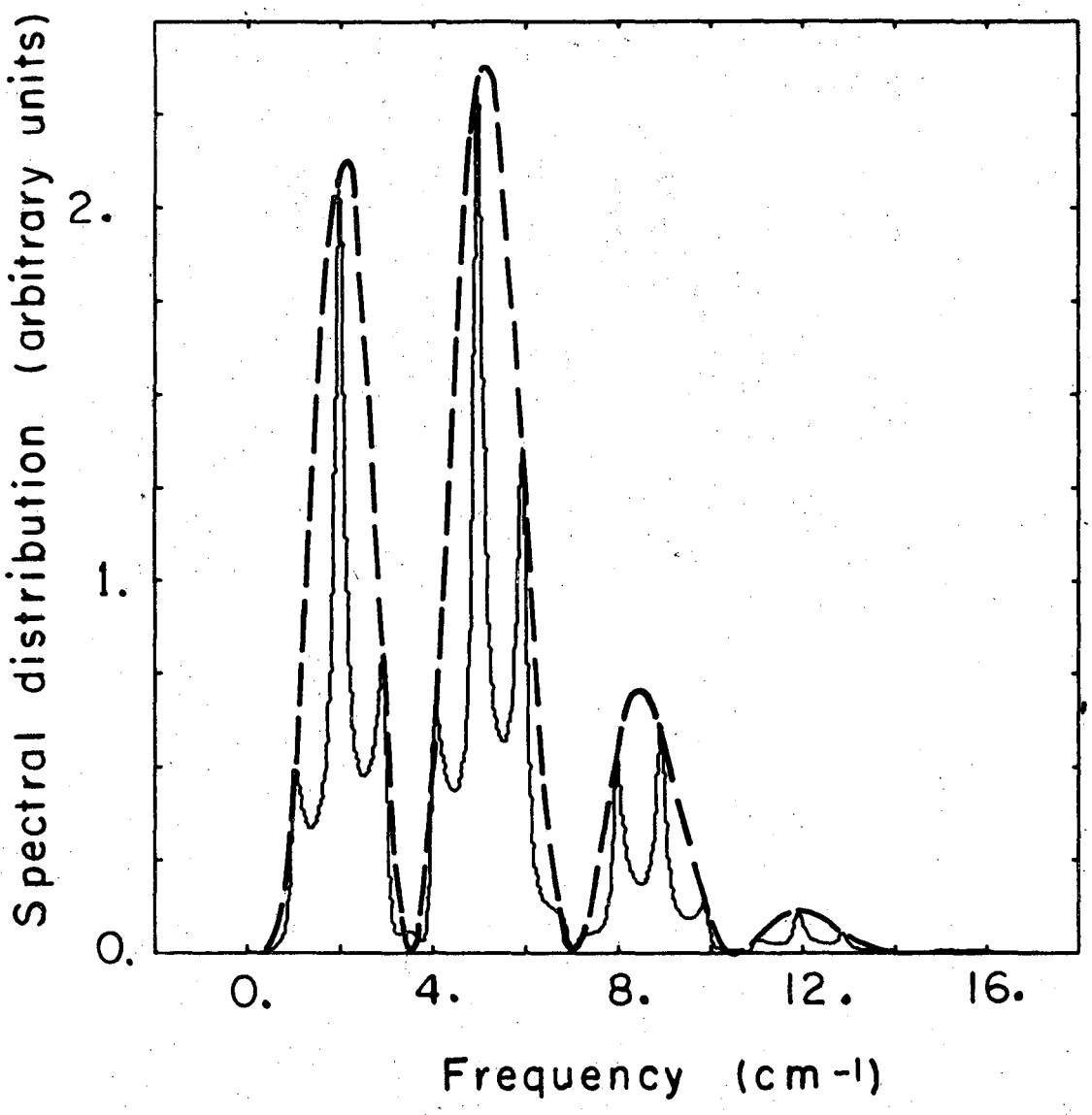

XBL709-3793

Fig. 12(a)

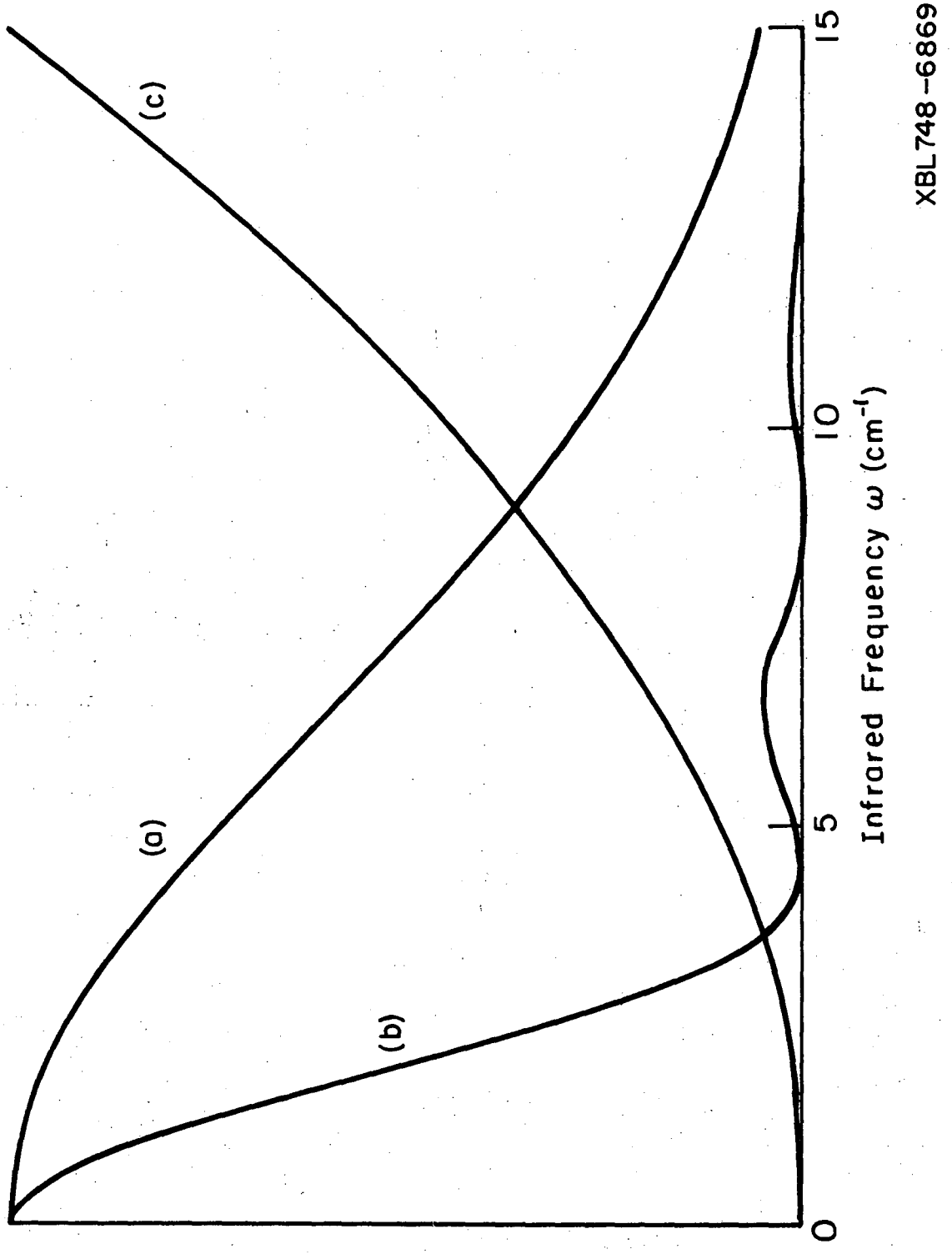

Fig. 12(b)

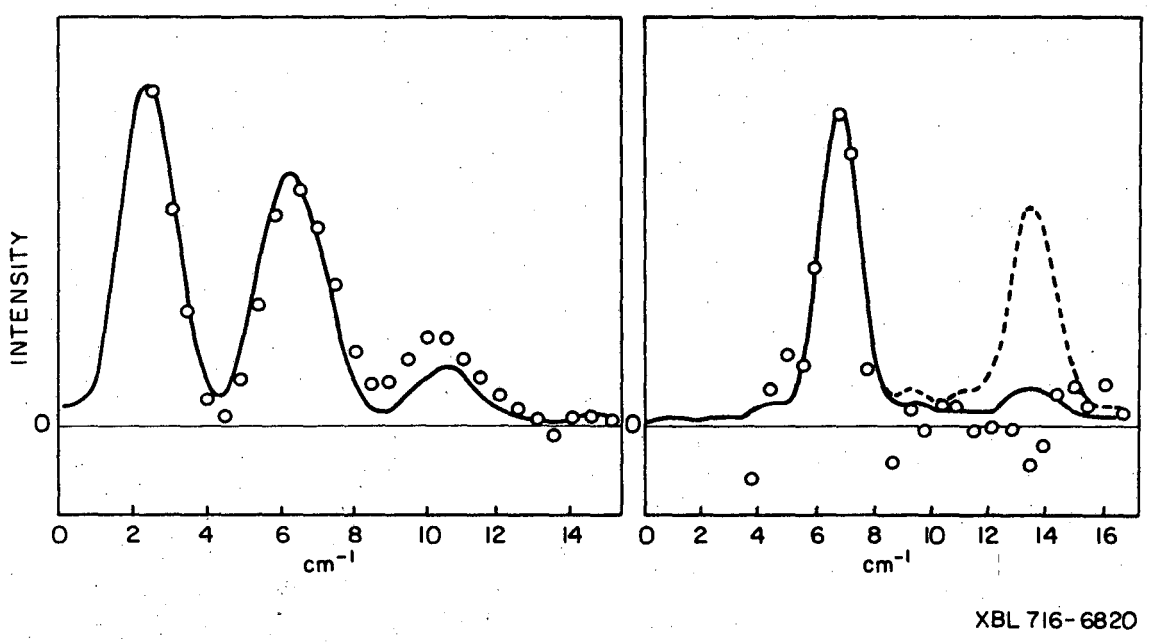
INTENSITY
0
0 2 4 6 8 10 12 14
cm⁻¹
0
0 2 4 6 8 10 12 14 16
cm⁻¹
XBL 716-6820

Fig. 13

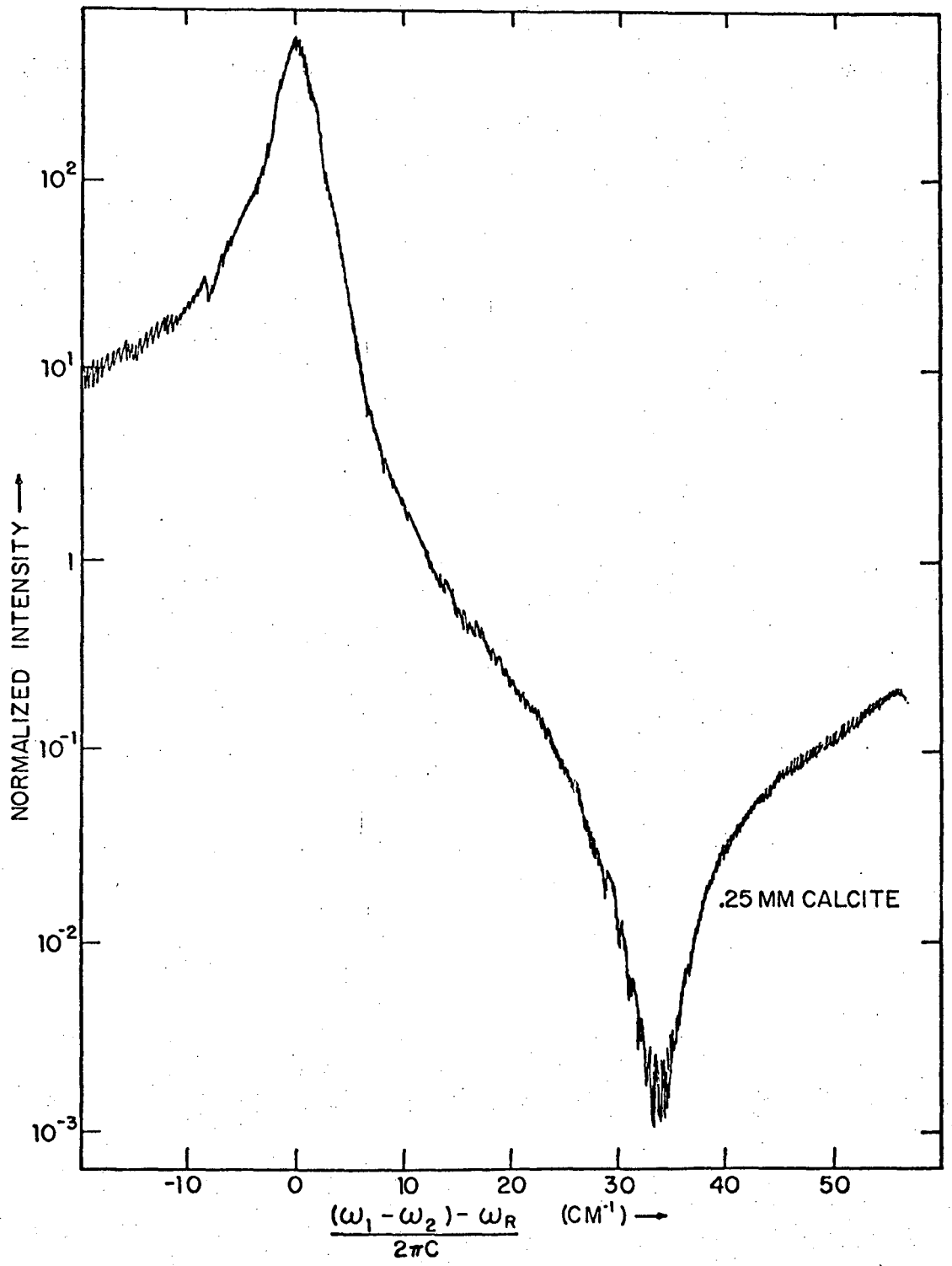

XBL 743-5809

Fig. 14

TABLE CAPTION

Table I. Present status of far-infrared generation by optical mixing in various cases. The output of a blackbody radiation source is also shown for comparison.

Technique	Mode of Operation	Input Laser Power	Peak IR Output	Average IR Output	Possible Tuning Range
Mixing of Visible Laser Beams in Solids	Pulsed	300 kW	200 mW at 50 cm^{-1}	6×10^{-8} W at 50 cm^{-1}	1 - 10,000 cm^{-1}
Mixing of CO_2 Laser Beams in Solids	Pulsed (2pps)	200 kW	200 mW at 100 cm^{-1}	10^{-7} W at 100 cm^{-1}	5 - 140 cm^{-1} in 3200 steps
	cw	25 W		10^{-7} W at 100 cm^{-1}	
Mixing via Spin-Flip Transitions	Pulsed (120 pps)	2 kW at ω_1 10 W at ω_2	2 μW at 100 cm^{-1}	5×10^{-11} W at 100 cm^{-1}	10 - 300 cm^{-1}
Mixing in Metal Vapor	Pulsed (10-100 pps)	1 kW at ω_1 10 kW at ω_2	100 mW at 2 μm	5×10^{-8} W at at 2 μm	100 - 5000 cm^{-1}
Stimulated Polariton Scattering	Pulsed	1 MW	5 W at 50 cm^{-1}	1.5×10^{-7} W at 50 cm^{-1}	40 - 200 cm^{-1}
Blackbody Source at 5000°K with 10 milli-sterad. Solid Angle and 1 cm^{-1} Spectral Content	cw			1.5×10^{-8} W at 50 cm-1	

Table I

LEGAL NOTICE

This report was prepared as an account of work sponsored by the United States Government. Neither the United States nor the United States Atomic Energy Commission, nor any of their employees, nor any of their contractors, subcontractors, or their employees, makes any warranty, express or implied, or assumes any legal liability or responsibility for the accuracy, completeness or usefulness of any information, apparatus, product or process disclosed, or represents that its use would not infringe privately owned rights.

TECHNICAL INFORMATION DIVISION
LAWRENCE BERKELEY LABORATORY
UNIVERSITY OF CALIFORNIA
BERKELEY, CALIFORNIA 94720